Surface-Emitting Laser—Its Birth and Generation of New Optoelectronics Field

Kenichi Iga, *Fellow, IEEE*

Invited Paper

***Abstract*—The surface-emitting laser (SEL) is considered one of the most important devices for optical interconnects and LANs, enabling ultra parallel information transmission in lightwave and computer systems. In this paper, we will introduce its history, fabrication technology, and discuss the advantages. Then, we review the progress of the surface-emitting laser and the vertical-cavity surface-emitting laser (VCSEL), covering the spectral band from infrared to ultraviolet by featuring its physics, materials, fabrication technology, and performances, such as threshold, output powers, polarizations, line-width, modulation, reliability, and so on.**

***Index Terms*—DBR, distributed Bragg reflector, gigabit ethernet, LAN, laser array, microlaser, microlens, multilayer, parallel transmission, quantum well, semiconductor laser, surface-emitting laser, vertical cavity laser, vertical-cavity surface-emitting laser.**

I. Introduction

WHAT IS THE surface-emitting laser (SEL) or the vertical cavity surface-emitting laser (VCSEL)? The structure is substantially different from conventional stripe lasers, i.e., the vertical cavity is formed by the surfaces of epitaxial layers and light output is taken from one of the mirror surfaces as shown in Fig. 1(a).

VCSEL [1], [2] looked to meet the third generation of development in 1999, as seen from Table I, as we entered a new information and technology era in 2000. The VCSEL is being applied in various optical systems, such as optical networks, parallel optical interconnects, laser printers, high density optical disks, and so on. We review its history and the progress of VCSELs in wide spectral ranges covered by various *III–V* compound semiconductors. Recent technologies and future prospects will be discussed.

We summarized the brief history of VCSEL research in Table I. It is recognized that the author suggested the device of VCSEL in 1977, as shown in Fig. 1(b). The first device came out in 1979, where we used a 1300-nm wavelength GaInAsP–InP material for the active region [3]. In 1986, we made a 6-mA threshold GaAs device [4] and then employed the metal organic chemical vapor deposition (MOCVD). The

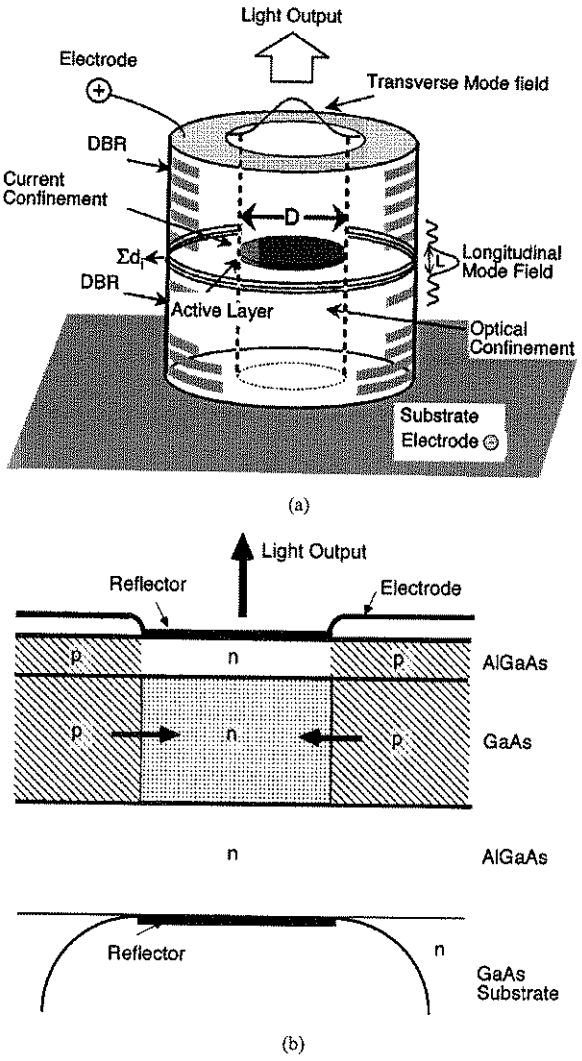

Fig. 1. Model of VCSEL. (a) Current model. (b) Initial idea.

first room-temperature continuous-wave (CW) device using GaAs material was demonstrated in 1988 [5]. In 1989, Jewell demonstrated a GaInAs VCSEL exhibiting a 1–2-mA threshold [6]. These two experiments encouraged the audience to be getting up at the stage of vertical-cavity surface-emitting laser research. Submilliampere threshold devices were demonstrated

Manuscript received July 13, 2000. This work was supported by the Ministry of Education, Science, Sport, and Culture with a Grant from COE Program 07CE2003.

The author is with the P&I Microsystem Research Center, Tokyo Institute of Technology, 4259 Nagatsuta, Midoriku, Yokohama 226-8503, Japan.

Publisher Item Identifier S 1077-260X(00)11545-X.

TABLE I
HISTORY OF VCSEL RESEARCH

I	1977-	First Idea and Initial Demonstrations
II	1988-	CW and Device Feasibility Study
III	1999-	Production and Extension of Applications

by improving the active region and distributed Bragg reflectors (DBRs).

Since 1992, VCSELs based on GaAs have been extensively studied [7]–[9] and some 780, 850, and 980-nm devices are now commercialized into optical systems. We improved a 1500-nm VCSEL [10] demonstrated a 1300-nm room-temperature CW device [11]. A wafer fusion technique enabled us to operate 1550-nm VCSELs at higher temperatures [12]. In 1993, a room-temperature high-performance CW red AlGaInAs device was demonstrated [13]. Since 1996, green-blue-ultraviolet device research was started [14], [15]. Since 1999, VCSEL-based optical transmitters have been introduced into gigabit per second LANs.

The initial motivation of SEL invention was a fully monolithic fabrication of laser cavity. Based upon this concept, the current issues include high speed modulation capability at very low-power consumption level, reproducible array production, and inexpensive moduling.

The VCSEL structure may provide a number of advantages as follows:

1) ultralow threshold operation is expected from its small cavity volume, reaching microampere levels;
2) $(I - I_{\rm th})I_{\rm th} > 100$ is possible, where I = driving current and $I_{\rm th}$ = threshold current;
3) wavelength and thresholds are relatively insensitive against temperature variation;
4) dynamic single-mode operation is possible;
5) large relaxation frequency provides high-speed modulation capability;
6) long device lifetime is due to completely embedded active region and passivated surfaces;
7) high-power conversion efficiency, i.e., >50%;
8) vertical emission from substrate;
9) easy coupling to optical fibers due to good mode matching from single mode through thick multimode fibers;
10) a number of laser devices can be fabricated by fully monolithic processes yielding very low cost chip production;
11) the initial probe test can be performed before separating devices into discrete chips;
12) easy bonding and mounting;
13) cheap modules and package cost;
14) densely packed and precisely arranged two-dimensional (2-D) laser arrays can be formed;
15) vertical stack integration of multithin-film functional optical devices can be made intact to the VCSEL resonator, taking the advantage of micromachining technology and providing polarization independent characteristics;
16) compatible integration together with LSIs.

In this paper, we would like to review the progress of VCSELs in a wide range of optical spectra based on GaInAsP, AlGaInAs, GaInNAs, GaInAs, GaAlAs, AlGaInP, ZnSe, GaInN, and other materials.

II. BASICS OF VCSEL

A. Threshold Current

The physical difference between VCSELs and conventional stripe geometry lasers is summarized in Table II. The major points are that the cavity length of VCSELs is in the order of wavelength which is much smaller than that of stripe lasers, having about a 300-μm wavelength and several micrometers of lateral size. Those provide us with substantial differences in laser performances.

We would like to discuss the threshold current of VCSELs. The threshold current $I_{\rm th}$ of SELs can be expressed by the equation with threshold current density $J_{\rm th}$

$$I_{\rm th} = \pi(D/2)^2 J_{\rm th} = \frac{eVN_{\rm th}}{\eta_i \tau_s} \cong \frac{eVB_{\rm eff}}{\eta_i \eta_{\rm spon}} N_{\rm th}^2 \qquad (1)$$

where e is electron charge. V is the volume of active region, which is given by

$$V = \pi(D/2)^2 d. \qquad (2)$$

The threshold carrier density is given by

$$N_{\rm th} = N_t + \frac{\alpha_a + \alpha_d + \alpha_m}{A_0 \xi}. \qquad (3)$$

The parameters used are defined as follows, where

α_a absorption loss coefficient averaged per unit length;
α_d diffraction loss coefficient averaged per unit length;
α_m mirror loss coefficient;
A_0 gain coefficient expressing differential gain $A_0 = dg/dN$, with g as the optical gain per centimeters;
$B_{\rm eff}$ effective recombination coefficient;
d total active layer thickness;
D diameter of active region;
L effective cavity length, including spacing layers and penetration layers of Bragg reflectors;
N_t transparent carrier density;
τ_p photon lifetime in cavity;
τ_s recombination lifetime;
ξ optical energy confinement factor, $\xi = \xi_t \xi_l$;
ξ_t transverse confinement factor;
ξ_l longitudinal confinement factor or filling factor relative to stripe lasers $\xi_l = d/L$ (for thick active layer) $\xi_l = 2d/L$ (for thin active layer, which is located at the loop of optical standing wave);
η_i injection efficiency, sometimes referred as internal efficiency;
$\eta_{\rm spon}$ spontaneous emission efficiency.

As seen in (1), we recognize that it is essential to reduce the volume of active region in order to decrease the threshold current. Assume that the threshold carrier density does not change that much. If we reduce the active volume, we can decrease the threshold as we make a small active region. We compare the dimensions of surface-emitting lasers and conventional stripe ge-

TABLE II
COMPARISON OF PARAMETERS BETWEEN STRIPE LASER AND VCSEL

Parameter	Symbol	Stripe Laser	Surface Emitting Laser
Active layer Thickness	d	100Å-0.1μm	80Å-0.5μm
Active Layer Area	S	$3\times300\mu m^2$	$5\times5\ \mu m^2$
Active Volume	V	$60\mu m^3$	$0.07\ \mu m^3$
Cavity Length	L	300μm	≈1μm
Reflectivity	R_m	0.3	0.99-0.999
Optical Confinement	ξ	≈3%	≈4%
Optical Confinement (Transverse)	ξ_t	3-5%	50-80%
Optical Confinement (Longitudinal)	ξ_l	50%	2×1%×3 (3QW's)
Photon Lifetime	τ_p	≈1 ps	≈1 ps
Relaxation Frequency (Low Current Levels)	f_r	<5GHz	>10GHz

ometry lasers in Table II. Notice that the volume of VCSELs could be $V = 0.06\ \mu m^3$, whereas the stripe lasers remain $V = 60\ \mu m^3$. This directly reflects the threshold current: the typical threshold of stripe lasers ranges from microampere or higher, while that for VCSEL is less than microampere due to a simple carrier confinement scheme, such as proton bombardment. It could even be as low as microampere by implementing sophisticated carrier and optical confinement structures, as will be introduced later.

An early stage estimation of threshold showed that the threshold current can be reduced in proportion to the square of the active region diameter. However, there should be a minimum value originating from the decrease of optical confinement factor that is defined by the overlap of optical mode field and gain region when the diameter is becoming small. In addition, the extreme minimization of volume, in particular, in the lateral direction, is limited by the optical and carrier losses due to optical scattering, diffraction of lightwave, nonradiative carrier recombination, and other technical imperfections.

B. Output Power and Quantum Efficiency

Also, we discuss the differential quantum efficiency of the VCSEL. If we use a nonabsorbing mirror for the front reflector, the differential quantum efficiency η_d from the front mirror is expressed as

$$\eta_d = \frac{\alpha_m}{\alpha_a + \alpha_d + \alpha_m} = \eta_i \frac{(1/L)\ln(1/R_f)}{\alpha + (1/L)\ln\left(1/\sqrt{R_f R_r}\right)} \quad (4)$$

where α is the total internal loss $(=\alpha_a + \alpha_d)$ and R_f and R_r are front and rear mirror reflectivities.

The optical power output is expressed by

$$\begin{aligned} P_o &= \eta_d \eta_{\text{spon}} C E_g I, \qquad (I \le I_{\text{th}}) \\ &= \eta_d E_g (I - I_{\text{th}}) + \eta_d \eta_{\text{spon}} C E_g I_{\text{th}}, \qquad (I \ge I_{\text{th}}) \end{aligned} \quad (5)$$

where

E_g is bandgap energy;
C is spontaneous emission factor;
I is driving current.

On the other hand the power conversion efficiency η_P far above threshold is given by

$$\eta_P = \frac{P_o}{V_b I} = \eta_d \frac{E_g}{V_b}\left(1 - \frac{I_{\text{th}}}{I}\right) \quad (6)$$

where V_b is bias voltage and the spontaneous component has been neglected. In the case of surface-emitting laser, the threshold current could be very small and therefore, the power conversion efficiency can be relatively large, i.e., higher than 50%. The power conversion efficiency is sometimes called wall-plug efficiency.

The modulation bandwidth is given by

$$f_{3\,\text{dB}} = 1.55 f_r \quad (7)$$

where f_r denotes the relaxation frequency, which is expressed by the equation

$$f_r = \frac{1}{2\pi\tau_s}\sqrt{\frac{\tau_s}{\tau_p}\left(\frac{I}{I_{\text{th}}} - 1\right)}. \quad (8)$$

The photon lifetime τ_p is given by

$$\tau_p = \frac{n_{\text{eff}}/c}{\alpha + \alpha_m}. \quad (9)$$

The photon lifetime is normally in the order of psec, which can be made slightly smaller than stripe lasers. Since the threshold current can be very small in VCSELs, the relaxation frequency could be relatively higher than the stripe lasers even in low driving ranges. The threshold carrier density N_{th} can

be expressed in terms of photon lifetime, which represents the cavity loss and given by using (3) and (9);

$$N_{\rm th} = N_t + \frac{1}{(c/n_{\rm eff})} \times \frac{1}{(dg/dN)} \times \frac{1}{\xi} \times \frac{1}{\tau_p}. \qquad (10)$$

It is noted that the threshold carrier density can be small if we make the differential gain dg/dN, the confinement factor ξ, and the photon lifetime τ_p large.

C. Criteria for Confirmation of Lasing

When we face a new or ultralow threshold device to check the lasing operation, the existence of a break from the linear increase of light output versus injection current (I–L) characteristic is an easy observation. Sometimes a nonlinearity is observed in the I–L characteristic but this does not necessarily mean laser oscillation. Even with a nonlasing sample nonlinearity is owed to the "filtering effect," electron-hole plasma emission, and nonradiating floor. The methods used to confirm the laser operation of vertical cavity, for example, are as follows:

1) break or kink in (L–I) characteristic;
2) narrow spectral linewidth <1 Å;
3) difference of near field pattern (NFP) and far field pattern (FFP) between the emissions below and above the threshold;
4) linearly polarized light of the emission above the threshold.

III. Device Design and Material

A. Device Configuration

As already shown in Fig. 1(a), the structure common to most VCSELs consists of two parallel reflectors, which sandwich a thin active layer. The reflectivity necessary to reach the lasing threshold normally should be higher than 99.9%. Together with the optical cavity formation, the scheme for injecting electrons and holes effectively into a small volume of active region is necessary for the current injection device. The ultimate threshold current depends on how to make the active volume small, as introduced in the previous section, and how well the optical field can be confined within the cavity to maximize the overlap with active region. These confinement structures will be presented in the later sections.

B. Materials

We show some material choices for VCSELs in Fig. 2. We list problems below that should be considered when making VCSELs, as discussed in the previous section:

1) design of resonant cavity and mode-gain matching;
2) multilayered DBRs to realize high reflective mirrors;
3) optical losses such as Auger recombination, intervalence band absorption, scattering loss, and diffraction loss;
4) p-type doping to reduce the resistivity in p-type materials for CW and high efficiency operation (if we wish to form multilayer DBRs, this will become much more severe);
5) heat sinking for high-temperature and high-power operation;

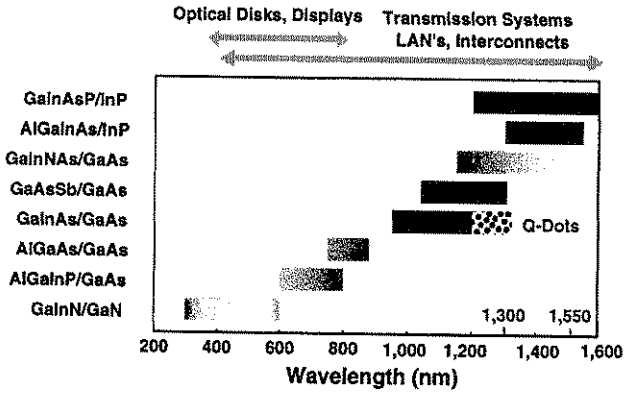

Fig. 2. Materials for VCSELs in wide spectral bands.

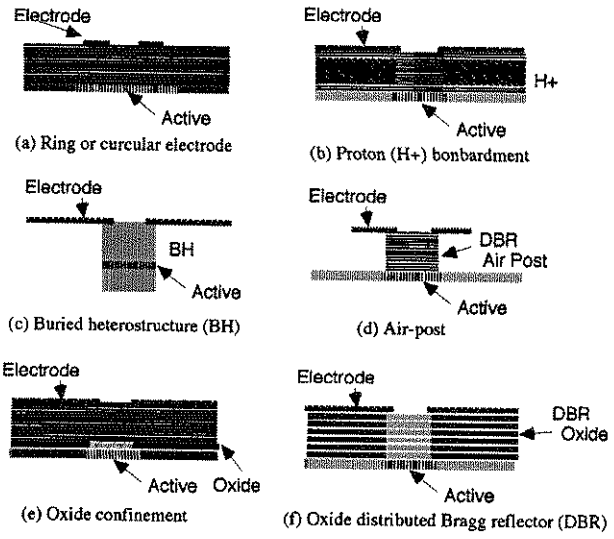

Fig. 3. Structures for current confinement.

6) catastrophic optical damage (COD) level is very important for high power operation;
7) crystal growth at reasonably high temperatures (e.g., higher than half of the melting temperatures).

C. Current Injection Scheme

Let us consider the current confinement for VCSELs. In Fig. 3, we show typical models of current confinement schemes reported so far.

a) Ring or circular electrode type: This structure can limit the current flow in the vicinity of the ring electrode. The light output can be taken out from the center window. This is easy to fabricate, but the current can not be confined completely within a small area due to diffusion.
b) Proton bombardment type: We make an insulating layer by proton (H^+) irradiation to limit the current spreading toward the surrounding area. The process is rather simple, and most of commercialized devices are made by this method.
c) Buried heterostructure (BH) type: We bury the mesa, including the active region, with a wide-gap semiconductor

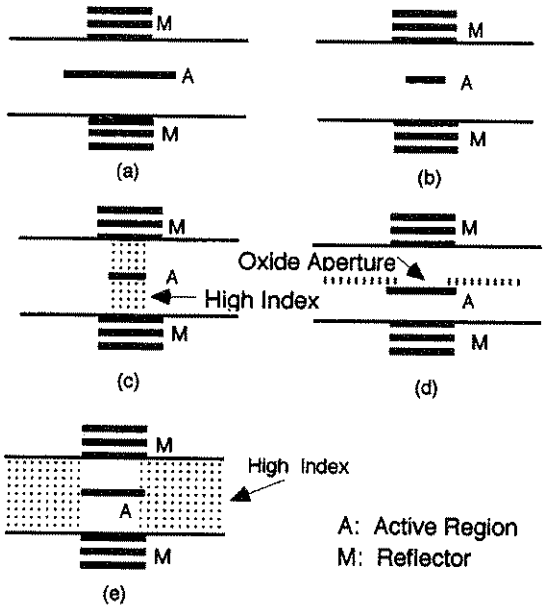

Fig. 4. Structures for optical confinement.

to limit the current. The refractive index can be small in the surrounding region, resulting in the formation of an index-guiding structure. This is an ideal structure in terms of current and optical confinement. The problem is that the necessary process is rather complicated, particularly, in making a tiny three-dimensional (3-D) device.

d) Air-post type: The circular or rectangular air-post is used to make a current confinement. This is the simplest way for device fabrication, although nonradiative recombination at the outer wall may deteriorate the performance.
e) Selective AlAs oxidation type: We oxidize the AlAs layer to make a transparent insulator.
f) Oxidized DBR type: The same method as above is applied to oxidize DBR, consisting of AlAs and GaAs. This is only one volume confinement method that can reduce the nonradiative recombination.

By developing new process technology, we could reach the laser performance, which is expected from the theoretical consideration.

D. Optical Guiding

The optical confinement schemes developed for VCSELs are introduced in Fig. 4. The fundamental concept is to increase the overlap of optical field with gain region.

a) Fabry–Perot type: The optical resonant field is determined by the two reflectors forming the plane that is parallel to the Fabry–Perot resonator. The diffraction loss increases if the mirror diameter gets too small.
b) Gain-guide type: We simply limit the field at the region where the gain exists. The mode may be changed at higher injection levels due to spatial hole burning.
c) BH: As introduced in the previous section, an ideal index guiding can be formed.
d) Selective AlAs oxidation type: Due to the index difference between AlAs and the oxidized region, we can confine the optical field as well by a lens effect.
e) Antiguiding type: The index is designed to be lower in the surrounding region in order to make a so-called antiguiding scheme. The threshold is rather high, but this structure is good for stable mode in high driving levels.

E. Transverse and Longitudinal Mode

The resonant mode in most SELs can be expressed by the well known Fabry–Perot TEM mode. The NFP of fundamental mode can be given by the Gaussian function

$$E = E_0 \exp\left[-\tfrac{1}{2}(r/s)^2\right] \tag{11}$$

where

E optical field;
r lateral distance;
s denotes spotsize.

The spotsize of normal SELs is several micronmeters, and relatively large when compared with stripe lasers, i.e., 2–3 μm. In the case of multimode operation, the mode behaves like the combination of multiple TEM_{pq}. The associated spectrum is broadened due to different resonant wavelengths.

FFP associated with Gaussian near field can be expressed by Gaussian function; spreading angle $\Delta\theta$ is given by

$$2\Delta\theta = 0.64(\lambda/2s). \tag{12}$$

Here, if $s = 3$ μm and $\lambda = 1$ μm, then $\Delta\theta = 0.05$ (rad) $= \cong 3°$. This kind of angle is narrower than conventional stripe lasers.

F. Polarization Mode

The VCSEL generally has linear polarization without exception. This is due to a small amount of asymmetric loss coming from the shape of the device or material. The device grown on a (100)-oriented substrate polarizes in (110) or equivalent orientations. The direction can not be identified definitely, and sometimes switches over due to spatial hole burning or temperature variation. In order to stabilize the polarization mode, special care should be taken. This issue will be discussed later.

IV. Surface-Emitting Laser in Long-Wavelength Band

A. GaInAsP–InP VCSEL

The first SEL device was demonstrated by using GaInAsP–InP system in 1978 and published in 1979 [3]. The importance of 1300- or 1550-nm devices is currently increasing because parallel lightwave systems are really needed to meet rapid increase of information transmission capacity in LANs. However, the GaInAsP–InP system, which is conventionally used in trank communication systems with the help of temperature controller, has some substantial difficulties for making VCSELs due to the following reasons.

1) Auger recombination and inter-valence band absorption (IVBA) are noticeable.
2) Index difference between GaInAsP and InP is relatively small to make DBR mirrors.
3) Conduction band offset is small.

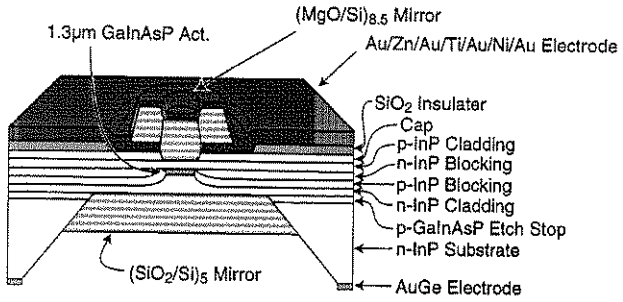

Fig. 5. 1300-nm VCSELs with thermally conductive dielectric DBR.

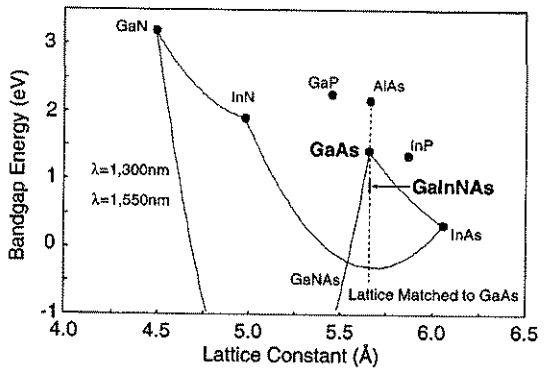

Fig. 6. Bandgap versus lattice-constant diagram.

Two hybrid mirror technologies are being developed. One uses a semiconductor/dielectric reflector [10]. Thermal problems for CW operation are extensively studied. A MgO–Si mirror with good thermal conductivity was demonstrated and achieved the first room-temperature CW operation with 1300 nm surface-emitting lasers, as shown in Fig. 5 [11]. Better results have been obtained by using Al_2O_3–Si mirrors [16].

The other is an epitaxial bonding of GaInAsP–InP active region and GaAs–AlAs mirrors, where a 144 °C pulsed operation was achieved by optical pumping. The AlAs–GaAs mirror has advantages in both electrical and thermal conductivity. CW threshold of 0.8 mA [17] and maximum operating temperature of up to 69 °C [12] have been reported for 1550-nm VCSELs with double-bonded mirrors [17]. More recently, the maximum operation was achieved at 71 °C [18]. In 1998, a tandem structure of 1300-nm VCSEL optically pumped by a 850-nm VCSEL has been demonstrated to achieve 1.5 mW of output power [19]. However, the cost of wafer consumption in wafer fusion devices may become the final bottleneck of low-cost commercialization.

Recently, a GaAsSb QW on GaAs substrate has been demonstrated for the purpose of 1300-nm VCSELs [20]. An AlGaAsSb–GaAs system has been found to form a good DBR [21]. Tunnel junction and AlAs oxide confinement structures may be very helpful for long-wavelength VCSEL innovation [22].

B. AlGaInAs–AlGaInAs VCSEL

The AlGaInAs lattice matched to InP is also considered. This system may exhibit a larger conduction band offset than the conventional GaInAsP system. Moreover, we can grow a thin AlAs layer to make the native oxide for a current confining aperture like the GaAs–AlAs system. The preliminary study has been made to demonstrate a stripe laser in our group, where a large T_0 was demonstrated. By using this system, the first monolithic VCSEL was fabricated, demonstrating room-temperature CW operation [23].

C. Long Wavelength VCSELs on GaAs Substrate

Another interesting system is GaInNAs lattice-matched to GaAs, as is shown in Fig. 6. This system has been pioneered by Kondow *et al.* [24] with a gas-source molecular-beam epitaxy (GSMBE). Also, $\lambda = 1190$-nm stripe lasers were fabricated, where the nitrogen content is 0.4%. Room-temperature CW operation of horizontal cavity lasers recently has been obtained, exhibiting the threshold current density of 1.5 kA/cm^2. Also, stripe geometry lasers were demonstrated with a threshold of 24 mA at room temperature [25]. It is reported that characteristic temperature is approximately 120K at room temperature [25]. If we can increase the nitrogen content up to 5%, the wavelength band of 1300–1550 nm may be covered. In particular, GaAs–AlAs Bragg reflectors can be incorporated on the same substrate, and AlAs oxidation is utilized [26]. Some consideration of device design was presented [27]. In any case, this system will substantially change the surface-emitting laser performances in the long wavelength range. Larson *et al.* first realized a VCSEL using this system [28].

The long-wavelength VCSEL formable on GaAs, as shown in Fig. 7 will have a great impact upon the realization of high performance devices. GaInNAs–GaAs is expected as a new material for long wavelength VCSELs. Every GaAs-based structure can be applied, and a large conduction band offset is expected. Some 1300-nm edge emitting lasers and a 1186-nm VCSELs were demonstrated. We achieved a lasing operation in GaInNAs edge emitters grown by chemical beam epitaxy (CBE), demonstrating $T_0 > 270$ K [29]. The $Ga_{1-x}In_xAs$ ternary substrate will be viable to make a high performance laser device by incorporating In = 0.25. Some sophisticated method to form this ternary substrate is attempted, $x = 0.1$ growing [30].

During the research of GaInNAs lasers, we found that a highly strained GaInAs–GaAs system containing large In-content (≅40%) can provide an excellent temperature characteristic [31], i.e., operating with $T_0 > 200$ K [32]. This system should be viable for $\lambda > 1200$-nm VCSELs for silica-fiber-based high-speed LANs [33].

A quantum dot structure is considered as a long-wavelength active layer on a GaAs substrate. A 1150-nm GaInAs-dot VCSEL was reported with a threshold current of 0.5 mA [73].

V. Surface Emitting Laser in Midwavelength Band

A. 980-nm GaInAs–GaAs VCSEL

The GaInAs–GaAs strained pseudomorphic system grown on a GaAs substrate emitting 0.98 μm of wavelength exhibits a high laser gain and has been introduced into SELs together with GaAs–AlAs multilayer reflectors [34]. A low threshold (≅1 mA at CW) has been demonstrated by Jewell *et al.* [6]. The threshold current of VCSELs has been reduced to submilliampere orders in various institutions of the world. Very low thresholds reported

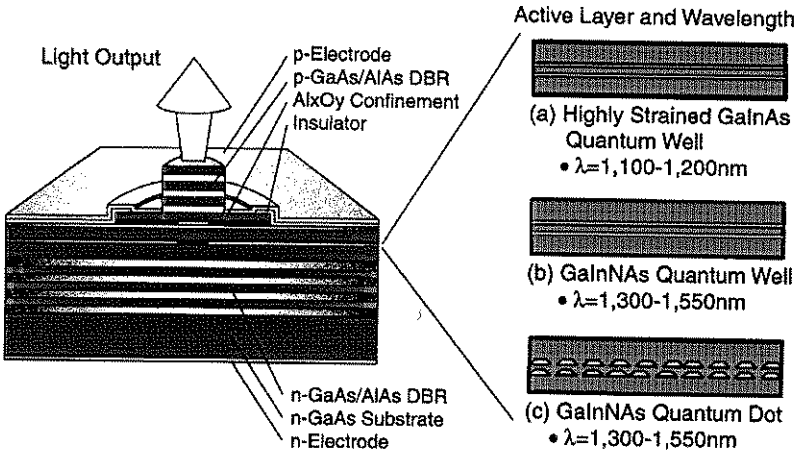

Fig. 7. Choices of long wavelength VCSELs formable on GaAs substrate.

before 1995 are 0.7 mA [7], 0.65 mA [8], and ≅0.2 mA [35]. Moreover, a threshold of 91 μA at room-temperature CW operation was reported by introducing the oxide current and optical confinement [36]. The theoretical expectation is less than 10 μA, if some good current and optical confinement structure can be introduced.

It has been made clear that the oxide aperture can function as a focusing lens since the central window has a higher index and the oxide region exhibits a lower index. This provide us with some phase shift to focus the light toward the center axis, which reduces the diffraction loss. The Al-oxide is effective both for current and optical confinements and solves the problems on surface recombination of carriers and optical scattering. We demonstrated 70 μA [37], [38] of threshold by using oxide DBR structure, 40 μA [39], and 8.5 μA [40].

In 1995, we developed a novel laser structure employing selective oxidizing process applied to AlAs, which is one member of the multilayer Bragg reflector. The schematic structure of the device now developed is shown in Fig. 8(a) [37], [38]. The active region is three quantum wells consisting of 80 Å GaInAs strained layers. The Bragg reflector consists of GaAs–AlAs quarter wavelength stacks of 24.5 pairs. After etching the epitaxial layers, including active layer and two Bragg reflectors, the sample was treated in a high-temperature oven with water vapor that had been bubbled by nitrogen gas. The AlAs layers are oxidized, preferentially with this process, and native oxide of Aluminum is formed at the periphery of etched mesas. It is recognized from SEM picture that only AlAs layers in DBR have been oxidized, as shown in Fig. 8(b) [41]. The typical size is 20-μm core starting from a 30-μm mesa diameter. We have achieved about 1 mW of power output and submicroampere threshold. The nominal lasing wavelength is 0.98 μm. We have made a smaller diameter device having 5 μm started from 20 μm mesa. The minimum threshold achieved is 70 μA at room temperature CW operation [38] as shown in Fig. 9. As the theoretically predicted, threshold is about 1 μA and this record may soon be cleared.

A relatively high power higher than 50 mW is becoming possible [42]. The power conversion efficiency 50% is reported.

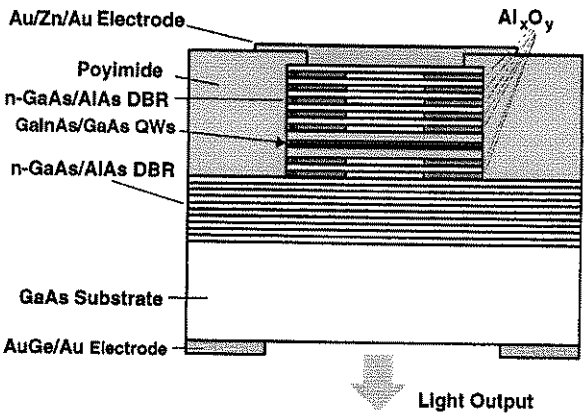

(a)

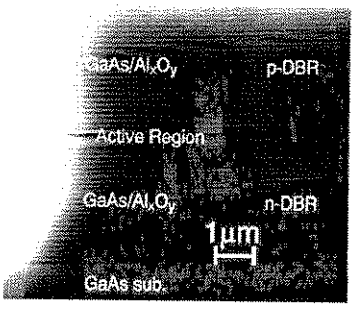

(b)

Fig. 8. (a) Schematic structure of oxide-confined GaInAs–GaAs VCSEL. (b) Oxidized AlAs layers in DBR.

[43]. Also, high efficiency operation at relatively low driving levels, i.e., a few milliamperes, became possible, which has been hard to achieve with stripe lasers. This is due to the availability of low resistive DBRs in corporation with Al-oxide aperture. In devices of about 1 μm in diameter, higher than 20% of power conversion efficiencies were reported [44], [45].

Regarding the power capability, near 200 mW has been demonstrated by a large size device in [46]. In a 2-D array involving 1000 VCSELs with active cooling, more than 2 W of CW output was achieved [47].

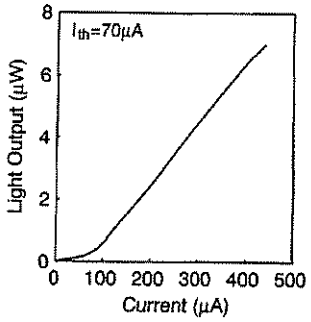

Fig. 9. Lasing characteristic showing the threshold of 70 μA.

In these low-power consumption devices, high-speed modulation is possible in low driving currents around 1 mA as well. This is substantially important in low-power interconnect applications enabling >10 Gb/s transmission or 1 Gb/s zero-bias operation [48]. Transmission experiments over 10 Gb/s and zero-bias transmission have been reported. We measured an eye diagram for 10 Gb/s transmission experiment through a 100-m multimode fiber [49].

Finally, VCSELs in this wavelength may find the market in 10 Gb LANs together with high-speed detectors and silica fibers. In any way, GaInAs VCSELs show the best performance, and the research to challenge the extreme characteristics will be continued.

B. 980-nm GaInAs–GaAs VCSEL on GaAs(311) Substrate

Most of VCSELs grown on GaAs (100) substrates show unstable polarization states due to isotropic material gain and symmetric cavity structures. VCSELs grown by MBE on GaAs (311) A substrates, however, show a very stable polarization state [50]. Also, trials of growth on (GaAs) B substrates by using MOCVD has been performed [51], [52]. Single transverse mode and polarization mode controlled VCSELs have not been realized at the same time.

In this section, we introduce a single transverse mode and polarization controlled VCSEL grown on a GaAs (311) B substrate. Both higher order transverse modes and a nonlasing orthogonal polarization modes are well suppressed with a suppression ratio of over 25 dB [53].

The schematic structure of a fabricated top-emitting VCSEL grown on GaAs (311) B is shown in Fig. 10(a), which has been grown by low pressure MOCVD [54]. The bottom n-type DBR consists of 36 pairs of $Al_{0.7}Ga_{0.3}As$–GaAs doped with Se. The top p-type DBR consists of 21 pairs of Zn-doped $Al_{0.7}Ga_{0.3}As$–GaAs and a 70-Å-thick AlAs carbon high-doping layer inserted at the upper AlGaAs interface by the carbon auto-doping technique proposed by us [41]. The active layer consists of three 8-nm-thick $In_{0.2}Ga_{0.8}As$ quantum wells and 10-nm GaAs barriers surrounded by $Al_{0.2}Ga_{0.8}As$ to form a cavity. An 80-nm-thick AlAs was introduced on the upper cavity spacer layer to form an oxide confinement. We oxidized the AlAs layer of etched 50 μm × 50 μm mesa at 480 °C for 5 min in an N_2–H_2O atmosphere by bubbling in 80 °C water and formed an oxide aperture of 2.5 μm × 3.0 μm.

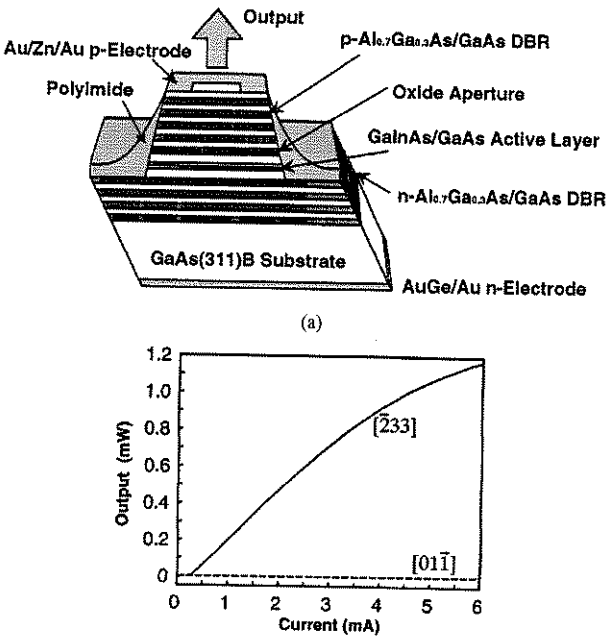

Fig. 10. InGaAs–GaAs VCSEL grown on (311) B substrate. (a) Device structure and (b) I–L characteristic exhibiting single mode and single polarization.

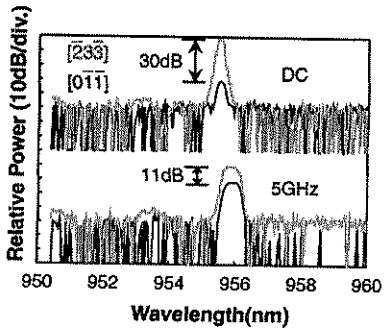

Fig. 11. Spectra of an oxide-confined InGaAs–GaAs VCSEL formed on (311) B substrate for dc and 5-Gb/s modulation conditions.

Fig. 10(b) shows a typical I–L and I–V characteristic under room-temperature CW operation. The threshold current is 260 mA, which is comparable to the lowest value reported for non(100)-substrate VCSELs. The threshold voltage is 1.5 V and the maximum output power is 0.7 mW at 4 mA.

In the entire tested driving range ($I < 16I_{th}$), a large side-mode suppression ratio (SMSR) of over 35 dB and an orthogonal polarization suppression ratio (OPSR) of over 25 dB were achieved at the same time. The single polarization operation was maintained at 5-GHz modulation condition [55], [56], as shown in Fig. 11.

The selective oxidation of AlAs is becoming a standard current and optical confinement scheme for milliampere threshold devices. The technology for mode-stable lasers using (311) B substrate is demonstrated for polarization control [56]. We have

obtained completely single-mode VCSEL by employing most of the available advanced techniques.

VI. Surface-Emitting Lasers in Near Infrared-Red Band

A. 850-nm GaAlAs–GaAs VCSEL

A GaAlAs–GaAs laser can employ almost the same circular buried hetero (CBH) structure as the GaInAsP–InP laser. In order to decrease the threshold, the active region is also constricted by the selective meltback method. In 1986, a threshold of 6 mA was demonstrated for the active region diameter ~6 μm under pulsed operation at 20.5 °C [4]. The threshold current density is about $J_{\rm th} \cong 200\ \mu A/\mu m^2$. It is noted that a microcavity of 7 μm long and 6 μm in diameter was realized.

The MOCVD grown CBH VCSEL was demonstrated by a two-step MOCVD growth and fully monolithic technology [57]. The first room-temperature CW operation was achieved in [5]. The lowest CW threshold current was 20 mA ($J_{\rm th} \cong 260\ \mu A/\mu m^2$). The differential quantum efficiency is typically 10%. The maximum CW output power is about 2 mW. The saturation of the output power is due to a temperature increase of the device. Stable single-mode operation is observed with neither subtransverse modes nor other longitudinal modes. The spectral linewidth above the threshold is less than 1 Å, which is limited by the resolution of the spectrometer. The mode spacing of this device was 170 Å. The side-mode suppression ratio (SMSR) of 35 dB is obtained at $I/I_{\rm th} = 1.25$. This is comparable to that of well designed DBR- or DFB-dynamic single-mode lasers.

Submilliampere thresholds and 10-mW outputs have been achieved. The power conversion efficiency of 57% has been demonstrated in [58]. Some commercial optical links have already been in markets. The price of low-skew multimode fiber ribbons may be a key issue for inexpensive multimode fiber-based data links.

As for the reliability of VCSELs, 10^7 hours of room-temperature operation is estimated, based upon the acceleration test at high temperature using proton-defined device [59]. In 1998, some preliminary test results were reported on oxide-defined devices, exhibiting no substantial negative failures.

B. 780-nm GaAlAs–GaAs VCSEL

The VCSEL in this wavelength was demonstrated in 1987 by optical pumping, and the first current injection device was developed by [9]. If we choose the Al content x to be 0.14 for $Ga_{1-x}Al_xAs$, the wavelength can be as short as 780 nm. This is common for compact disc lasers. When the quantum-well is used for active layer, blue shift should be taken into account.

We show the design below [60]. The active layer $Ga_{0.86}Al_{0.14}As$ is formed by a super lattice consisting of GaAs (33.9 Å), and AlAs (5.7 Å), with 14 period. The DBR is made of AlAs–$Al_{0.35}Ga_{0.65}As$–$Al_{0.3}Ga_{0.7}As$–$Al_{0.35}Ga_{0.65}As$ as 1 period. The n-DBR has 28.5 pair and p-DBR consists of 22 pairs. The threshold in 1991 was 4–5 mA and the output was 0.7–0.8 mW. Later on, the multiquantum wells (MQW) made of Al content ($x = 0.1/0.3$) was introduced, and the threshold of 200 μA and the output of 1.1 mW were demonstrated [60].

C. AlGaInP Red VCSEL

Generally, the light-emitting device in short wavelength regions may have more severe operation problems than longer wavelength regions since the photon energy is large and p-type doping is technically harder to perform. If aluminum is included in the system, the degradation due to Al-oxidation is appreciable. The AlGaInP–GaAs system, emitting red color ranging from 630–670 nm, is considered a laser for the first generation digital video disc system. GaInAlP–GaAs VCSELs are developed; room-temperature operation exhibiting submilliampere threshold, 8 mW output, and 11% conversion efficiency have been obtained [59]. The wavelength is 6720 nm with oxide aperture of 2 μm × 3 μm. The threshold is 0.38 mA, the output is 0.6 mW, and the maximum operation temperature is 85 °C [12]. In 1998, submilliampere thresholds, 11% power conversion efficiency, 8 mW of output power were achieved [61].

VII. Surface-Emitting Lasers in Green–Blue UV Band

Visible SELs are extremely important for disk, printers, and display applications. In particular, red, green, and blue surface emitters may provide much wider technical applications, if realized. The ZnSe system is the material to provide CW operation of green-blue semiconductor lasers that operate over 1000 hours. It is supposed to be good for green lasers, and the MOCVD may be a key for getting reliable devices in mass production. We have developed a simple technique to get a high p-doping by an ampule diffusion of LiN to ZnSe. Also, a dielectric mirror deposition was investigated, and relatively high reflectivity was obtained to provide an optical pumped vertical cavity. Some trials regarding optical pumped and current-injection surface-emitting lasers have been made [14].

GaN and related materials can cover wide spectral ranges green to UV. The reported reliability of GaN-based LEDs and LDs [62], [63] seems to indicate a good material potentiality for SELs as well.

Optical gain is one of the important parameters to estimate the threshold current density of GaN-based VCSELs [64]. The estimation of linear gain for GaN–$Al_{0.1}Ga_{0.9}N$ quantum well is carried out using the density-matrix theory with intraband broadening. The transparent carrier density of GaN is higher than other III–V materials like as GaAs, presumably originating from its heavy electron and hole masses. Generally, the effective masses of electrons and holes depend on the bandgap energy. Thus, it seems that the wide-bandgap semiconductors require higher transparent carrier densities than narrow-bandgap materials. The introduction of quantum wells for wide-bandgap lasers is very effective. This result indicates that the GaN–$Al_{0.1}Ga_{0.9}N$ quantum well is useful for low threshold operation of VCSELs [65].

The trial for realizing green to UV VCSELs has just began. Some optical pumping experiments have been reported [14], [15]. It is necessary to establish some process technologies for device fabrication, such as etching, surface passivation, substrate preparation, metallization, current confinement formation, and so on [65]. We have made a preliminary study to search for dry etch of a GaN system by a chlorine-based reactive ion beam etch, which was found to be possible.

The GaN system has large potentialities for short wavelength lasers. AlN–GaN DBR and ZrO–SiO_2 DBR are formed for VCSELs [64], and some selective growth techniques have been attempted. A photo-pumped GaInN VCSEL was reported [15]. Also, we are trying to grow GaInN–GaN on silica glass for large-area light emitters [66].

VIII. Innovating Technologies

A. Targeting Characteristics

By overcoming any technical problems, such as making tiny structures, ohmic resistance of electrodes, and improving heat sinking, we believe that we can obtain a 1-μA device. A lot of effort toward improving the characteristics of SELs have been made, including surface passivation in the regrowth process for BH, microfabrication, and fine epitaxies.

As introduced before, very low thresholds of around 70, 40, and about 10 μA were reported by employing the aforementioned oxidation techniques. Therefore, by optimizing the device structures, we can expect a threshold lower than microamperes in the future [67].

The efficiency of devices is another important issue for various applications. By introducing the oxide confinement scheme, power conversion efficiency has been drastically improved due to the effective current confinement and the reduction of optical losses. Also, the reduction of driving voltage by innovating the contacting technology helped a lot. As introduced earlier, higher than 57% of power conversion efficiency, sometimes called wall-plug efficiency, has been realized. A noticeable difference of the conventional stripe laser is that high efficiency can be obtained at relatively low driving ranges in the case of VCSELs. Therefore, further improvement may enable us to achieve highly efficient arrayed devices, which have not been attained in any other type of lasers.

The high-speed modulation capability is very essential for communication applications. In VCSELs, 10-Gb/s or higher modulation experiments have been reported. For VCSEL systems, it is a great advantage that over 10-Gb/s modulation is possible at around 1-mA driving levels. This characteristic is preferable for low-power consumption optical interconnect applications [68].

The final screening for applicability of any component and system is reliability of devices. A high-temperature acceleration life test of proton-implanted VCSELs showed an expected room-temperature lifetime of over 10^7 hours [59]. There is no reason why we can not have very long-life devices by VCSELs, since the active region is completely embedded in wide-gap semiconductor materials and the mirror is already passivated.

The lasing performance of VCSELs will be improved by optimizing and solving the following issues: 1) improvement of crystal quality; 2) quantum structures (strain, wire/dot, modulation doping); 3) polarization control; 4) wavelength control; and 5) high-power and low-operation voltage.

Microetching technology is inevitable for making reproducible arrayed VCSELs. We have prepared ICP (inductively coupled plasma) etching for well-controlled and low-damage etch of GaAs and InP systems [69].

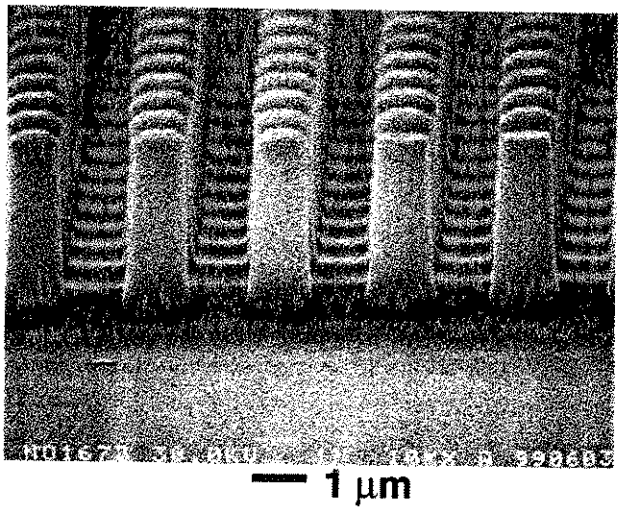

Fig. 12. SEM picture of InP microstructure by ICP etching.

An example of scanning electron microscope (SEM) picture of an etched InP system for microcavity structure is shown in Fig. 12. In order to further achieve substantial innovations in SEL performances, the following technical issues remain unsolved or nonoptimized:

1) AlAs oxidation and its application to current confinement and optical beam focusing [70], [71];
2) Modulation doping, p-type, and n-type modulation doping to quantum wells/barriers;
3) Quantum wires and dots for active engines [72], [73];
4) Strained quantum wells and strain compensation;
5) Angled substrates, such as (311A), (311B), (411);
6) New material combinations such as GaInNAs–GaAs for long wavelength emission;
7) Wafer-fusion technique to achieve optimum combination of active region and mirrors;
8) Transparent mirrors to increase quantum efficiency and output power;
9) Multiquantum barriers to prevent carrier leakage to p-cladding layer;
10) Tunnel junction.

Among them, the AlAs oxidation technology seems to be the most important technology to confine the current to reduce the threshold. Moreover, the oxidized layer works to give some amount of phase shift to focus the beam providing index guiding cavity.

A tunnel junction was introduced in SELs [74]. Recently, the reverse tunnel junction began to be utilized for effective carrier injection [22] and a noble self-aligned current aperture was proposed, as shown in Fig. 13 [22].

B. Polarization Steering

A wide variety of functions, such as polarization control, amplification, and detection, can be integrated along with SELs by stacking. The polarization control will become very important for VCSELs [75]. One method incorporates a grating terminator to a DBR. The other method includes the utilization of

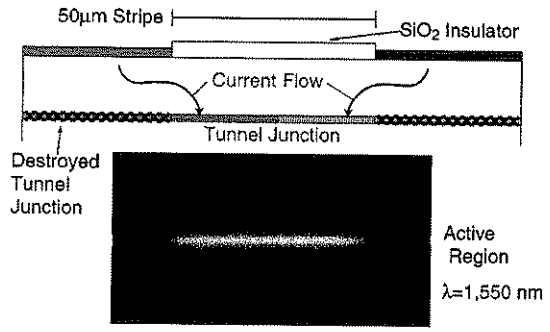

Fig. 13. Scheme of parallel fiber-optic module based on surface-emitting laser array.

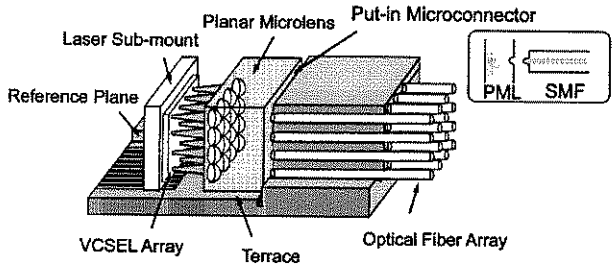

Fig. 14. MOB concept to ease the assembling of components without precise alignment.

quantum wires [72] and off-angled substrate, where we can differentiate the optical gain between one lateral direction and the perpendicular direction [50]. As already introduced, reasonably low threshold and well controlled polarization behaviors have been demonstrated by (311)A and (311)B substrates. The device formation on (311)B GaAs substrates employing MOCVD methods has been attempted by solving the difficulties of crystal growth and p-type doping. We have achieved 260 μA of CW threshold, single transverse, and single polarization operation. OPSR of about 30 dB was obtained. In Fig. 11 we show the spectra of a (311) B-based InGaAs–GaAs VCSEL under dc and a 5-Gb/s modulation condition [56]. At a high-speed modulation condition, some deterioration of OPSR was observed. The physical understanding is not clear at this moment and is open to question. In any way, the use of angled substrates, which provide us with differential gain in two orthogonal polarizations, will be very effective for controlling the polarization independent of structures and the size of devices.

IX. VCSEL-Based Integration Technology

A wide variety of functions, such as frequency tuning, amplification, and filtering, can be integrated along with SELs by stacking. Another possible way of moduling is to use the micro-optical bench concept [76] to ease the assembling of components without precise alignment, as shown in Fig. 14. Moreover, a 2-D parallel optical-logic system can deal with a large amount of image information with high speed. To this demand, an SEL will be a key device. Optical neural chips have been investigated for the purpose of making optical neurocomputers and vertical to surface transmission electro-photonic (VSTEP) integrated device [77].

High power capabilities from VCSELs are very interesting because they feature largely extending 2-D arrays. For the purpose of realizing coherent arrays, a coherent coupling of these arrayed lasers has been tried by using a Talbot cavity and considering phase compensation. It is pointed out that 2-D arrays are more suitable to make a coherent array than a linear configuration since we can take the advantage of 2-D symmetry. The research activity is now forwarded to monolithic integration of VCSELs, taking the advantage of small-cavity dimensions. A densely packed array has also been demonstrated for the purpose of making high-power lasers and coherent arrays.

Also, there are now attempts to integrate surface-operating photonic elements using quantum wells, such as an optical switch, frequency tuner, optical filter, and super-lattice functional devices. Monolithic lenses can be formed on VCSELs by an etching process to narrow the beam divergence [78].

X. VCSEL Applications

Lastly, we consider some possible applications, including optical interconnects, parallel fiber-optic subsystems, etc. We summarized possible application areas of VCSELs in Table III.

We performed an experiment of > 10-Gb/s modulation of VCSELs and transmission via 100-m multimode fibers. The BER is shown in Fig. 15 [79]. Long-wavelength VCSELs should be useful for silica-based fiber links that provide ultimate transmission capability by taking advantage of single-wavelength operation and massively parallel integration. The development of 1200–1550-nm VCSELs may be one of the most important issues in SEL research [79].

The red-color VCSEL emitting 650 nm can match the low-loss band of plastic fibers. Short-distance data links are considered by using 1-mm diameter plastic fibers with a developed graded index. This system provides us with very easy optical coupling, and VCSELs can very nicely match this application.

By taking advantage of wide-band and small-volume transmission capability, the optical interconnect is considered to be inevitable in computer technology. A parallel interconnect scheme is wanted and new concepts are being researched. Vertical optical interconnect of LSI chips and circuit boards may be another interesting issue. New architecture for a 64-channel interconnect has been proposed and a modeling experiment was performed using GaInAs VCSEL arrays [80].

Several schemes for optical computing have been considered, but one of the bottlenecks may be a lack of suitable optical devices, in particular, 2-D VCSELs and surface-operating switches. Fortunately, very low threshold VCSELs have been developed, and stack integration together with 2-D photonic devices are now considered.

Green to UV VCSELs will be useful in the optoelectronics field as in ultra-high density optical memories. We proposed a model of optical pickup [81] using VCSEL in Fig. 16. This kind of simple pickup is now commercialized. A near-field optics scheme is considered to realize high-density optical memories [82]. In Fig. 17, a possible device was demonstrated [83], which

TABLE III
APPLICATIONS OF VCSELS

Technical Fields	Systems
1. Optical Communications	LANs, Optical links, Mobile links, etc.
2. Computer Optics	Computer links, Optical interconnects, High speed/Parallel data transfer, etc.
3. Optical Memory	CD, DVD, Near field, Multi-beam, Initializer, etc.
4. Optoelectronic Equipments	Printer, Laser pointer, Mobile tools, Home appliances, etc.
5. Optical Information Processing	Optical processors, Parallel processing, etc.
6. Optical Sensing	Optical fiber sensing, Bar code readers, Encoders, etc.
7. Displays	Array light sources, Multi-beam search-lights,
8. Illuminations	High efficiency sources, Micro illuminators, , etc. Adjustable illuminations, etc.

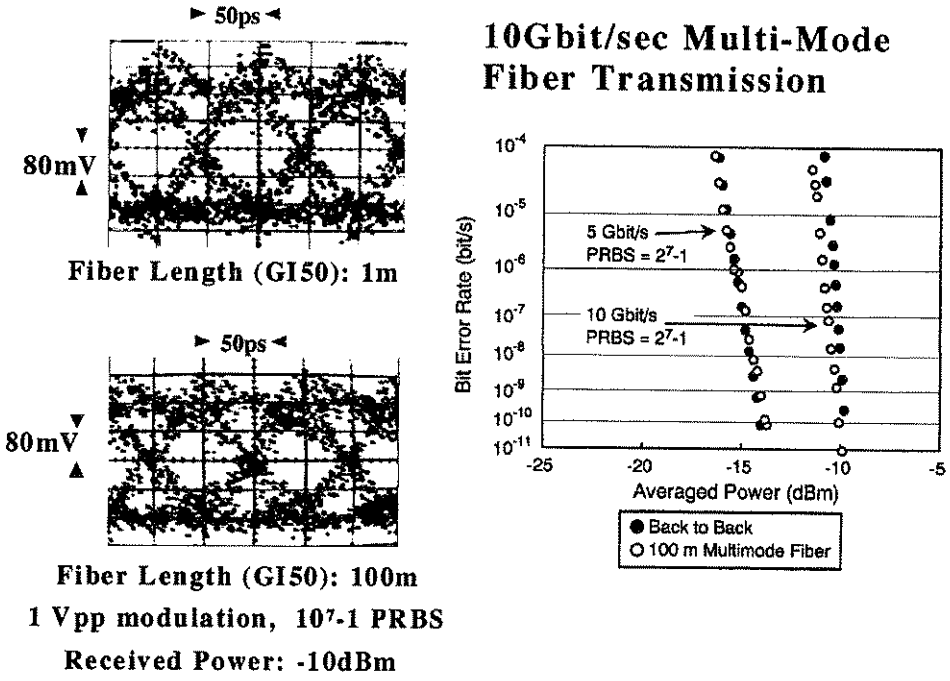

Fig. 15. BER of high-speed modulation of VCSELs transmitted via 100-m-long multimode fibers.

is useful for full-color flat displays and large-area projectors, illuminations and light signals, light decorations, UV lithography, laser processes, medical treatment, etc.

XI. SUMMARY

The technology for SELs has been developed and high-performance devices have began to be realized. Threshold current below 10–100 μA was demonstrated and extremely low thresholds lower than 1 μA are the target of research. Reasonably high-power >200 mW and power-conversion efficiency >57% are also demonstrated, which are equivalent to or better than conventional stripe lasers.

Long-wavelength devices are facing some difficulties with high temperature and large output, but there are several innovating technologies to open up the bottlenecks. Very short-wavelength lasers may cultivate wider applications if realized. The SEL is now considered a key component in ultra-low-power consumption and high-power applications over any other semiconductor laser.

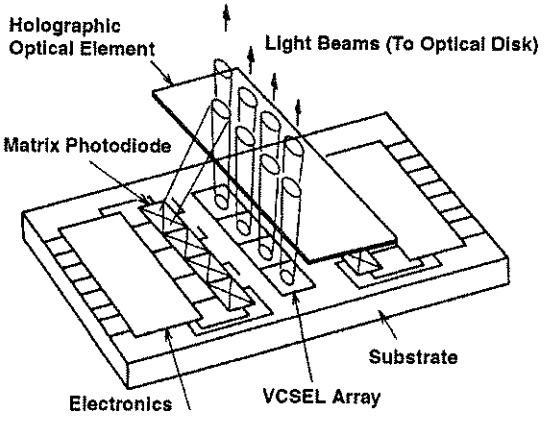

Fig. 16. Idea of optical pickup using surface-emitting laser.

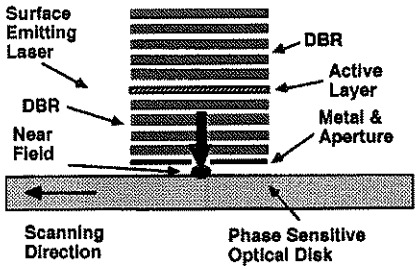

Fig. 17. VCSEL for the generation of optical near field using nano-aperture.

Vertical optical interconnects of LSI chips and circuit boards and multiple fiber systems may be the most interesting field related to VCSELs. From this point of view, the device should be as small as possible. The future process technology for it, including epitaxy and etching, will drastically change the situation of VCSELs. Some optical technologies are already introduced in various subsystems and, in addition, the arrayed microoptic technology would be very helpful for advanced systems.

The most promising application will be gigabit LANs. GaAs VCSELs emitting 850 nm of standardized wavelength are mass produced for >1–Gb/s LAN and simple optical links. For high-end systems, 1300–1550-nm devices are requested. By using VCSEL and micromachining technology, we demonstrated a temperature-insensitive surface normal Fabry–Perot filter for add–drop filtering in WDM. To establish an appropriate module technology utilizing VCSELs, an MOB has been investigated together with planar microlens array. Related to planar microlens array application and ultra-parallel information processing, an image recognition system is investigated using synthetic discriminant function (SDF) filtering.

In summary, the ultra-parallel optoelectronics based upon arrayed devices, including VCSELs, will open up a new era for the 2000 millennium.

ACKNOWLEDGMENT

The author would like to thank Prof. F. Koyama, T. Miyamoto, and other laboratory members for their collaboration and assistance in preparing the original drawings.

REFERENCES

[1] K. Iga, F. Koyama, and S. Kinoshita, "Surface emitting semiconductor laser," *IEEE J. Quant. Electron.*, vol. 24, pp. 1845–1855, Sept. 1988.

[2] K. Iga, "Surface emitting laser," *Trans. IEICE, C-I*, vol. JBI-C-1, no. 9, pp. 483–493, Sept. 1998.

[3] H. Soda, K. Iga, C. Kitahara, and Y. Suematsu, "GaInAsP/InP surface emitting injection lasers," *Jpn. J. Appl. Phys.*, vol. 18, pp. 2329–2330, Dec. 1979.

[4] K. Iga, S. Kinoshita, and F. Koyama, "Microcavity GaAlAs/GaAs surface-emitting laser with I_{th} = 6 mA," *Electron. Lett.*, vol. 23, no. 3, pp. 134–136, Jan. 1987.

[5] F. Koyama, S. Kinoshita, and K. Iga, "Room-temperature continuous wave lasing characteristics of GaAs vertical cavity surface-emitting laser," *Appl. Phys. Lett.*, vol. 55, no. 3, pp. 221–222, July 1989.

[6] J. L. Jewell, S. L. McCall, A. Scherer, H. H. Houh, N. A. Whitaker, A. C. Gossard, and J. H. English, "Transverse modes, waveguide dispersion and 30-ps recovery in submicron GaAs/AlAs microresonators," *Appl. Phys. Lett.*, vol. 55, pp. 22–24, July 1989.

[7] R. Geels and L. A. Coldren, "Narrow-linewidth, low threshold vertical-cavity surface-emitting lasers," in *12th IEEE Int. Semiconductor Laser Conf.*, vol. B-1, 1990, pp. 16–17.

[8] T. Wipiejewski, K. Panzlaf, E. Zeeb, and K. J. Ebeling, "Submilliamp vertical cavity laser diode structure with 2.2-nm continuous tuning," in *18th European Conf. Opt. Comm. '92*, Sept. 1992, PDII-4.

[9] Y. H. Lee, B. Tell, K. F. Brown-Goebeler, R. E. Leibenguth, and V. D. Mattera, "Deep-red continuous wave top-surface-emitting vertical-cavity AlGaAs superlattice lasers," *IEEE Photon. Technol. Lett.*, vol. 3, no. 2, pp. 108–109, Feb. 1991.

[10] T. Miyamoto, T. Uchida, N. Yokouchi, Y. Inaba, F. Koyama, and K. Iga, "A study on gain-resonance matching of CBE grown $l = 1.5$ μm surface emitting lasers," *IEEE/LEOS Annu.*, no. DLTA13.2, p. 542, Nov. 1992.

[11] T. Baba, Y. Yogo, K. Suzuki, F. Koyama, and K. Iga, "Near room temperature continuous wave lasing characteristics of GaInAsP/InP surface emitting laser," *Electron. Lett.*, vol. 29, no. 10, pp. 913–914, May 1993.

[12] D. I. Babic, K. Streubel, R. P. Mirin, J. Pirek, N. M. Margalit, J. E. Bowers, E. L. Hu, D. E. Mars, L. Yang, and K. Carey, "Room temperature performance of double-fused 1.54 μm vertical-cavity lasers," in *IPRM 96*, Apr. 1996, no. ThA1-2.

[13] K. D. Choquette, R. P. Schneider, M. H. Crawford, K. M. Geib, and J. J. Figiel, "Continuous wave operation of 640–660 nm selectively oxidised AlGaInP vertical cavity lasers," *Electron. Lett.*, vol. 31, pp. 1145–1146, July 1995.

[14] K. Iga, "Possibility of Green/Blue/UV surface emitting lasers," in *Int. Symp. Blue Laser Light Emitting Diodes*, Mar. 1996, Th-11, pp. 263–266.

[15] T. Someya, K. Tachibana, Y. Arakawa, J. Lee, and T. Kamiya, "Lasing oscillation in InGaN vertical cavity surface emitting lasers," in *16th Int. Semiconductor Laser Conf.*, 1998, PD-1, pp. 1–2.

[16] S. Uchiyama, N. Yokouchi, and T. Ninomiya, "Room-temperature CW operation of 1.3-μm GaInAsP SL-MQW surface emitting laser," in *43th Spring Meeting Jpn. Soc. Appl. Phys.*, 1996, 26p-C-7.

[17] N. M. Margalit, D. I. Babic, K. Streubel, R. P. Mirin, R. L. Naone, J. E. Bowers, and E. L. Hu, "Submilliamp long wavelength vertical cavity lasers," *Electron. Lett.*, vol. 32, p. 1675, Aug. 1996.

[18] K. A. Black, N. M. Margalit, E. R. Hegblom, P. Abraham, Y.-J. Chiu, J. Piprek, J. E. Bowers, and E. L. Hu, "Double-fused 1.5 μm vertical cavity lasers operating continuous wave up to 71 °C," in *16th Int. Semiconductor Laser Conf.*, 1998, ThA8, pp. 247–248.

[19] V. Jayaraman, J. C. Geske, M. H. MacDougal, F. H. Peters, T. D. Lowes, and T. T. Char, "Uniform threshold current, continuous-wave, single mode 1300 nm vertical cavity lasers from 0 to 70 °C," *Electron. Lett.*, vol. 34, no. 14, pp. 1405–1407, July 1998.

[20] M. Yamada, T. Anan, K. Kurihara, K. Nishi, K. Tokutome, A. Kamei, and S. Sugou, "Room temperature low threshold CW operation of 1.23 μm GaAsSb VCSELs of GaAs substrates," *Electron. Lett.*, vol. 36, no. 7, pp. 637–638, Mar. 2000.

[21] E. Hall, G. Almuneau, J. K. Kim, O. Sjölund, H. Kroemer, and L. A. Coldren, "Electrically-pumped, single-epitaxial VCSELs at 1.55 μm with Sb-based mirrors," *Electron. Lett.*, vol. 35, no. 16, pp. 1337–1338, Aug. 1999.

[22] S. Sekiguchi, T. Miyamoto, T. Kimura, F. Koyama, and K. Iga, "Self-arraigned current confinement structure using AlAs/InP tunnel junction in GaInAsP/InP semiconductor lasers," *Appl. Phys. Lett.*, vol. 75, no. 11, pp. 1512–1514, Sep. 1999.

[23] C. Kazmierski, J. P. Debray, R. Madani, N. Bouadma, J. Etrillard, I. Sagnes, F. Alexandre, and M. Quillec, "First all-monolithic VCSELs on InP : +55 °C pulse lasing at 1.56 μm with GaInAlAs/InP system," in *16th Int. Semiconductor Laser Conf.*, 1998, PD-3, pp. 5–6.

[24] M. Kondow, K. Nakahara, T. Kitatani, Y. Yazawa, and K. Uomi, "GaInNAs laser diode pulsed operation at 77 K," in *OECC'96*, 18D-3-2.

[25] K. Nakahara, M. Kondow, T. Kitatani, M. C. Larson, and K. Uomi, "1.3-μm continuous-wave lasing operation in GaInNAs quantum-well lasers," *IEEE Photon. Technol. Lett.*, vol. 10, pp. 487–488, Apr. 1998.

[26] K. Iga, "Vertical cavity surface emitting lasers based on InP and related compounds—Bottleneck and corkscrew," in *Conf. Indium Phosphide Related Materials*, Schwabisch Gmund, Germany, Apr. 1996.

[27] T. Miyamoto, K. Takeuchi, F. Koyama, and K. Iga, "Novel GaInNAs/GaAs quantum well structure for long wavelength semiconductor lasers," *IEEE Photon. Technol. Lett.*, vol. 9, pp. 1448–1450, Nov. 1997.

[28] M. C. Larson, M. Kondow, T. Kitatani, K. Nakahara, K. Tamura, H. Inoue, and K. Uomi, "Room-temperature pulsed operation of GaInNAs/GaAs long-wavelength vertical cavity lasers," in *IEEE/LEOS'97*, Nov. 1997, no. PD1.3.

[29] T. Kageyama, T. Miyamoto, S. Makino, N. Nishiyama, F. Koyama, and K. Iga, "High-temperature operation up to 170 °C of GaInNAs–GaAs quantum-well lasers grown by chemical beam epitaxy," *IEEE Photon. Technol. Lett.*, vol. 12, pp. 10–12, Jan. 2000.

[30] H. Ishikawa, K. Otsubo, and H. Imai, "Experimental and theoretical analysis of the temperature performance of high T_0 lasers on InGaAs ternary substrate," in *16th IEEE Int. Semiconductor laser Conf.*, Oct. 1998, TuE51, pp. 195–196.

[31] D. Schlenker, T. Miyamoto, Z. Chen, F. Koyama, and K. Iga, "1.17 μm highly strained GaInAs–GaAs quantum-well laser," *IEEE Photon. Technol. Lett.*, vol. 11, pp. 946–948, Aug. 1999.

[32] Z. Chen, D. Schlenker, T. Miyamoto, T. Kondo, M. Kawaguchi, F. Koyama, and K. Iga, "High-temperature characteristics of near 1.2 μm InGaAs/AlGaAs lasers," *Jpn. J. Appl. Phys.*, vol. 38, no. 10B, pp. L1178–1179, Oct. 1999.

[33] F. Koyama, S. Schlenker, T. Miyamoto, Z. Chen, A. Matsutani, T. Sakaguchi, and K. Iga, "1.2 μm highly strained GaInAs/GaAs quantum-well lasers for single-mode fibre datalink," *Electron. Lett.*, vol. 35, no. 13, pp. 1079–1081, June 1999.

[34] T. Sakaguchi, F. Koyama, and K. Iga, "Vertical cavity surface emitting laser with and AlGaAs/AlAs Bragg reflector," *Electron. Lett.*, vol. 24, no. 15, pp. 928–929, July 1988.

[35] T. Numai, T. Kawakami, T. Yoshikawa, M. Sugimoto, Y. Sugimoto, H. Yokoyama, K. Kasahara, and K. Asakawa, "Record low threshold current in microcavity surface-emitting laser," *Jpn. J. Appl. Phys.*, vol. 32, no. 10B, pp. L1533–L1534, Oct. 1993.

[36] D. L. Huffaker, D. G. Deppe, C. Lei, and L. A. Hodge, "Sealing AlAs against oxidative decomposition and its use in device fabrication," in *CLEO'96*, Anaheim, no. JTuH5.

[37] Y. Hayashi, T. Mukaihara, N. Hatori, N. Ohnoki, A. Matsutani, F. Koyama, and K. Iga, "Lasing characteristics of low-threshold oxide confinement InGaAs–GaAlAs vertical-cavity surface-emitting lasers," *IEEE Photon. Technol. Lett.*, vol. 7, pp. 1234–1236, Nov. 1995.

[38] ——, "Record low threshold index-guided InGaAs/GaAlAs vertical-cavity surface-emitting laser with a native oxide confinement structure," *Electron. Lett.*, vol. 31, no. 7, pp. 560–561, Mar. 1995.

[39] D. L. Huffaker, J. Shin, and D. G. Deppe, "Low threshold half-wave vertical-cavity lasers," *Electron. Lett.*, vol. 30, pp. 1946–1947, Nov. 1994.

[40] G. M. Yang, M. MacDougal, and P. D. Dupkus, "Ultralow threshold current vertical cavity surface emitting lasers obtained with selective oxidation," *Electron. Lett.*, vol. 31, pp. 886–888, May 1995.

[41] N. Hatori, A. Mizutani, N. Nishiyama, F. Motomura, F. Koyama, and K. Iga, "P-type delta doped InGaAs/GaAs quantum well vertical-cavity surface-emitting lasers," *IEICE C-I*, vol. J81-C-I, no. 7, pp. 410–416, 1998.

[42] F. H. Peters, M. G. Peters, D. B. Young, J. W. Scott, B. J. Tibeault, S. W. Corzine, and L. A. Coldren, "High power vertical cavity surface emitting lasers," in *13th IEEE Semiconductor Laser Conf.*, 1992, PD-1, pp. 1–2.

[43] K. L. Lear, R. P. Schneider Jr., K. D. Choquette, S. P. Kilcoyne, and K. M. Geib, "Selectively oxidised vertical cavity surface emitting lasers with 50% power conversion efficiency," *Electron. Lett.*, vol. 31, pp. 208–209, Feb. 1995.

[44] K. D. Choquette, A. A. Allerman, H. Q. Hou, G. R. Hadley, K. M. Geib, and B. E. Hammons, "Improved efficiency of small area selectively oxidized VCSELs," in *16th Int. Semiconductor Laser Conf.*, Oct. 1998, ThA3, pp. 237–238.

[45] L. A. Coldren, E. R. Hegblom, and N. M. Margalit, "Vertical cavity lasers with record efficiency at small sizes using tapered apertures," in *16th Int. Semiconductor Laser Conf.*, Oct. 1998, PD-2, pp. 3–4.

[46] B. Weigl, G. Reiner, M. Grabherr, and K. J. Ebeling, "High-power selectively oxidized vertical-cavity surface-emitting lasers," in *CLEO'96*, Anaheim, June 1996, JTuH2.

[47] D. Francis, H.-I. Chen, W. Yuen, G. Li, and C. Chang-Hasnain, "Monolithic 2D-VCSEL array with 0.2 W CW output power," in *16th Int. Semiconductor Laser Conf.*, Oct. 1998, TuE3, pp. 99–100.

[48] B. J. Thibeault, K. Bertilsson, E. R. Hegblom, P. D. Floyd, and L. A. Coldren, "High-speed modulation characteristics of oxide-apertured vertical-cavity lasers," in *15th IEEE Int. Semicon. Laser Conf.*, 1996, M3.2, pp. 17–18.

[49] N. Hatori, A. Mizutani, N. Nishiyama, A. Matsutani, T. Sakaguchi, F. Motomura, F. Koyama, and K. Iga, "An over 10 Gb/s transmission experiment using p-type d-doped InGaAs/GaAs quantum-well vertical cavity surface-emitting laser," *IEEE Photon. Technol. Lett.*, vol. 10, pp. 194–196, Feb. 1998.

[50] M. Takahashi, N. Egami, T. Mukaihara, F. Koyama, and K. Iga, "Lasing characteristics of GaAs (311)A substrate based InGaAs/GaAs vertical cavity surface emitting lasers," *IEEE J. Select. Topics Quantum Electron.*, vol. 3, no. 2, pp. 372–378, Apr. 1997.

[51] K. Tateno, Y. Ohiso, C. Amano, A. Wakatsuki, and T. Kurokawa, "Growth of vertical-cavity surface-emitting laser structures on GaAs (311)B substrates by metalorganic chemical vapor deposition," *Appl. Phys. Lett.*, vol. 70, no. 25, pp. 3395–3396, June 1997.

[52] A. Mizutani, N. Hatori, N. Ohnoki, N. Nishiyama, N. Ohtake, F. Koyama, and K. Iga, "P-type doped AlAs growth on GaAs (311)B substrate using carbon auto-doping for low resistance GaAs/AlAs distributed Bragg reflectors," *Jpn. J. Appl. Phys.*, vol. 36, no. 11, pp. 6728–6729, Nov. 1997.

[53] A. Mizutani, N. Hatori, N. Nishiyama, F. Koyama, and K. Iga, "A low threshold polarization-controlled vertical cavity laser grown on GaAs (311) substrate," *IEEE Photon. Technol. Lett.*, vol. 10, pp. 633–635, May 1998.

[54] N. Nishiyama, A. Mizutani, N. Hatori, F. Koyama, and K. Iga, "Single mode and stable polarization InGaAs/GaAs surface emitting laser grown on GaAs (311)B substrate," in *16th Int. Semiconductor Laser Conf.*, 1998, ThA1, pp. 233–234.

[55] ——, "Single transversemode and stable polarization operation under high-speed modulation of InGaAs/GaAs vertical cavity surface emitting laser grown on GaAs (311)B substrate," *IEEE Photon. Technol. Lett.*, vol. 10, pp. 1676–1678, Dec. 1998.

[56] N. Nishiyama, A. Mizutani, N. Hatori, M. Arai, F. Koyama, and K. Iga, "Lasing characteristics of InGaAs/GaAs polarization controlled vertical-cavity surface emitting laser grown on GaAs (311) B substrate," *Select. Topics Quantum Electron.*, vol. 5, pp. 530–536, Feb. 1999.

[57] F. Koyama, K. Tomomatsu, and K. Iga, "GaAs surface emitting lasers with circular buried heterostructure grown by metalorganic chemical vapor deposition and two-dimensional laser array," *Appl. Phys. Lett.*, vol. 52, no. 7, pp. 528–529, Feb. 1988.

[58] R. Jager, M. Grabherr, C. Jung, R. Michalzik, G. Reiner, B. Weigl, and K. J. Ebeling, "57% wallplug efficiency oxide-confined 850 nm wavelength GaAs VCSELs," *Electron. Lett.*, vol. 33, no. 4, pp. 330–331, Feb. 1997.

[59] J. K. Guenter, R. A. Hawthorne, D. N. Granville, M. K. Hibbs-Brenner, and R. A. Morgan, "Reliability of proton-implanted VCSELs for data communications," *Proc. SPIE*, vol. 2683, p. 1, 1996.

[60] H.-E. Shin, Y.-G. Ju, H.-H. Shin, J.-H. Ser, T. Kim, E.-K. Lee, I. Kim, and Y. -H. Lee, "780 nm oxidised vertical-cavity surface-emitting lasers with $Al_{0.11}Ga_{0.89}As$ quantum wells," *Electron. Lett.*, vol. 32, no. 14, pp. 1287–1288, July 1996.

[61] M. H. Crawford, K. D. Choquette, R. J. Hickman, and K. M. Geib, "Performance of selectively oxidized AlGaInP-based visible VCSELs," *OSA Trends Optics Photon. Series*, vol. 15, pp. 104–105, 1998.

[62] S. Nakamura, M. Senoh, S. Nagahama, N. Iwasa, T. Yamada, T. Matsushita, H. Kiyoku, and Y. Sugimoto, "InGaN-based multi-quantum-well-structure laser diodes," *Jpn. J. Appl. Phys.*, pt. 2, vol. 35, no. 1B, pp. L74–L76, Jan. 1996.

[63] S. Nakamura, M. Senoh, S. Nagahama, N. Iwasa, T. Yamada, T. Matsushita, H. Kiyoku, Y. Sugimoto, T. Kozaki, H. Umemoto, M. Sano, and K. Chocho, "High-power, long-lifetime InGaN/GaN/AlGAN-based laser diodes grown on pure GaN substrates," *Jpn. J. Appl. Phys.*, vol. 37, pp. L309–L312, Mar. 1998.

[64] T. Sakaguchi, T. Shirasawa, N. Mochida, A. Inoue, M. Iwata, T. Honda, F. Koyama, and K. Iga, "Highly reflective AlN/GaN and ZrO_2/SiO_2 multilayer distributed Bragg reflectors for InGaN/GaN surface emitting lasers," in *LEOS 1998 11th Annual Meeting Conf. Proc.*, TuC4, Dec. 1998.

[65] T. Shirasawa, N. Mochida, A. Inoue, T. Honda, T. Sakaguchi, F. Koyama, and K. Iga, "Interface control of GaN/AlGaN quantum well structures in MOVPE growth," *J. Cryst. Growth*, pp. 124–127, 1998.

[66] Y. Moriguchi, T. Miyamoto, T. Sakaguchi, M. Iwata, Y. Uchida, F. Koyama, and K. Iga, "GaN polycrystal growth on silica substrate by metalorganic vapor phase epitaxy (MOVPE)," in *3rd Int. Symp. Blue Laser Light Emitting Diodes*, Berlin, Mar. 2000, WeP-19, p. 83.

[67] K. Iga and F. Koyama, "Surface emitting lasers," in *Academic Monthly*, Gakujyutsu-Geppo; JSPS ed., Jan. 1996, vol. 49, no. 1, pp. 42–46.

[68] B. E. Lemoff and L. A. Buckman, "Low-cost WDM transceivers for the LAN," in *Dig. LEOS-Summer Topical Meeting*, 1999, MA2.1, pp. 3–4.

[69] A. Matsutani, H. Ohtsuki, F. Koyama, and K. Iga, "C60 resist mask of electron beam lithography for chlorine-based reactive ion beam etching," *Jpn. J. Appl. Phys.*, vol. 37, no. 7, pp. 4211–4212, July 1998.

[70] D. G. Deppe, D. L. Huffaker, J. Shin, and Q. Deng, "Very-low-threshold index-confined planar microcavity lasers," *IEEE Photon. Technol. Lett.*, vol. 7, pp. 965–967, Sept. 1995.

[71] H. Bissessur, F. Koyama, and K. Iga, "Modeling of oxide-confined vertical cavity surface emitting lasers," *IEEE J. Quantum Electron.*, vol. 3, pp. 344–352, Apr. 1997.

[72] N. Hatori, T. Mukaihara, Y. Hayashi, N. Ohnoki, F. Koyama, and K. Iga, "Design and fabrication of InGaAs/GaAs quantum wires for vertical-cavity surface-emitting lasers," *Jpn. J. Appl. Phys.*, vol. 35, no. 3, pp. 1777–1778, Mar. 1996.

[73] D. G. Deppe, D. L. Huffaker, Q. Deng, T.-H. Oh, and L. A. Graham, "Oxide-confined VCSELs with quantum well quantum dot active region," in *IEEE/LEOS'97*, Nov. 1997, no. ThA 1, pp. 287–288.
[74] Y. Kotaki, S. Uchiyama, and K. Iga, "GaInAsP/InP surface emitting laser with two active layers," in *1984 Int. Conf. Solid-State Devices*, no. C-2-3.
[75] T. Mukaihara, N. Ohnoki, Y. Hayashi, N. Hatori, F. Koyama, and K. Iga, "Polarization control of vertical-cavity surface-emitting lasers using a birefringent metal/dielectric polarizer loaded on top distributed Bragg reflector," *IEEE J. Select. Topics Quantum Electron.*, vol. 1, pp. 667–673, June 1995.
[76] Y. Aoki, R. J. Mizuno, Y. Shimada, and K. Iga, "Parallel and bi-directional optical interconnect module using vertical cavity surface emitting lasers(VCSELs) and 3-D micro optical bench (MOB)," in *1999 IEEE/LEOS Summer Topical Meetings*, July 1999, WA2.4, pp. 9–10.
[77] T. Numai, M. Sugimoto, I. Ogura, H. Kosaka, and K. Kasahara, "Current versus light-output characteristics with no definite threshold in pnpn vertical to surface transmission electro-photonic devices with a vertical cavity," *Jpn. J. Appl. Phys.*, vol. 30, no. 4A, pp. L602–L604, Apr. 1991.
[78] K. Iga, T. Kambayashi, K. Wakao, C. Kitahara, and K. Moriki, "GaInAsP/InP double-structure planar LEDs," *IEEE Trans. Electron. Devices*, vol. ED-26, pp. 1227–1230, Aug. 1979.
[79] F. Koyama, D. Schlenker, T. Miyamoto, Z. Chen, A. Matsutani, T. Sakaguchi, and K. Iga, "Data transmission over single-mode fiber by using 1.2-mm uncooled GaInAs–GaAs laser for Gb/s local area network," *IEEE Photon. Technol. Lett.*, vol. 12, pp. 125–127, Feb. 2000.
[80] H. Kosaka, M. Kajita, Y. Li, and Y. Sugimoto, "A two-dimensional optical parallel transmission using a vertical-cavity surface-emitting laser array module and an image fiber," *IEEE Photon. Technol. Lett.*, vol. 9, pp. 253–255, Feb. 1997.
[81] K. Iga, "Surface operating electrooptic devices and their application to array parallel signal processing," in *ECOC'90*, vol. 2, Sept. 1990, WeB-2.1, pp. 895–932.
[82] K. Goto, "Tera bytes optical disk with electric tracking control using micro-cavity VCSEL array and PD array," in *Dig. LEOS-Summer Topical Meeting*, 1997, MC-4, pp. 21–22.
[83] T. Yamatoya, S. Mori, F. Koyama, and K. Iga, "Design and fabrication of high power and broad-band GaInAsP/InP strained quantum well superluminescent diodes with tapered active region," in *CLEO Pacific Rim'99*, July 1999, FO6v, pp. 1227–1228.

Kenichi Iga (S'67–M'68–SM'80–F'87) was born in Hiroshima Prefecture, Japan, in 1940. He received the B.E., M.E., Dr.Eng. degrees from the Tokyo Institute of Technology, Tokyo, Japan, in 1963, 1965, and 1968, respectively.

In 1968, he joined the P & I Laboratories, Tokyo Institute of Technology, where he became an Associate Professor in 1973 and Professor in 1984. Since 1993, he has been a Teiichi Yamazaki Chair Professor. He is currently the Director of Institute Library and the Director of P & I Microsystem Research Center. From 1979 to 1980, he was with Bell Laboratories as a Visiting Technical Staff Member. He is the author of many books, including *Fundamentals of Microoptics* (New York: Academic), *Fundamentals of Laser Optics* (New York: Plenum), *Introduction to Optical Fiber Communication* (New York: Wiley), and *Process Technology for Semiconductor Lasers* (New York: Springer-Verlag). He first proposed and pioneered the research of surface-emitting semiconductor lasers, which triggered research activities in surface-emitting lasers and has become very important as coherent light-sources with two-dimensional (2-D) parallelism. His research interests include microoptics, gradient-index microlens arrays, and the realization of 2-D arrayed optical devices in combination with surface-emitting lasers.

Prof. Iga is a Member of the Institute of Electronics, Information, and Communication Engineers of Japan (IEICE) and a Fellow of the Optical Society of America. He has served as an Asian Representative for the IEEE Lasers and Electro-Optics Society (IEEE/LEOS) from 1984 to 1990, CLEO Japanese Subcommittee Chair from 1988 to 1990, Board of Governor for IEEE/LEOS from 1991 to 1993, and President of the Electronics Society in 1996. He has received numerous awards, including the Inada Memorial Prize in 1966, IEICE Distinguished Book Award for *Introduction to Optical Fiber Communications* in 1978, the Sakurai Memorial Prize from the Optoelectronic Industry and Technology Development Association in 1987, IEE Premium Award in 1988, the William Streifer Award for Scientific Achievement in 1992, the Toray Award in 1995, the IEEE Third Millennium Medal, and the John Tyndall Awardin 1998.

APM VCSEL's

Vertical-Cavity Surface-Emitting Lasers: Design, Growth, Fabrication, Characterization

Jack L. Jewell, J. P Harbison, A. Scherer, Y. H. Lee, and L. T. Florez

Abstract—**We have designed, fabricated, and tested vertical-cavity surface-emitting lasers (VCSEL) with diameters ranging from 0.5 μm to >50 μm. The approaches we have taken have produced (not necessarily by us) the smallest, the lowest threshold, the highest quantum efficiency, and the highest modulation speed VCSEL's to date. The four principal sections of this paper—design issues, molecular beam epitaxial growth, fabrication, and lasing characteristics—are written by people who are closely involved in their development.**

I. Introduction

VERTICAL-CAVITY surface-emitting lasers (VCSEL) have optical cavities orthogonal to those of conventional edge-emitting diode lasers [1]. This simple change in the cavity orientation produces radical differences in the beam characteristics, scalability, optoelectronic design, fabrication, and array configurability. For example, VCSEL's typically emit circularly symmetric Gaussian beams in contrast to the astigmatic beams of edge emitters, and thus require no anamorphic correction. The smallest electrically pumped VCSEL's to date have active material volumes $<0.05\ \mu m^3$, an order of magnitude less than the smallest edge emitter [2], and optically pumped VCSEL's are as small as $0.002\ \mu m^3$ active volume. Electrical pumping in VCSEL's is, so far, not nearly as efficient as in edge emitters, because all demonstrated designs have compromised between optical and electronic characteristics. For this reason, edge emitters currently have a clear edge in high-power applications. VCSEL fabrication techniques differ widely depending on the laser size and, for example, whether or not a two-dimensional addressable array is being built. A two-dimensional addressable array is a configuration well suited for VCSEL's but extremely impractical for edge emitters. These widespread differences virtually assure each type of laser a portion of the diode laser market.

VCSEL's were pioneered by Iga *et al.* at the Tokyo Institute of Technology [3]. Starting in the late 1970's with an electrically pumped laser operating at 77 K emitting 1.2 μm wavelength [1], they later produced the first VCSEL arrays [4], devices with reasonably low thresholds [5], the first room-temperature CW VCSEL [6], and the first linewidth measurements of CW VCSEL's [7]. Industrial adoption of this technology produced the first low-threshold room-temperature CW VCSEL [8]. The VCSEL's in our work evolved from all-optical GaAs nonlinear Fabry–Perot etalons originally designed for optical bistability [9] and switching at Bell Laboratories, also in the late 1970's. Starting with films of GaAs a few microns thick and coated with dielectric mirrors [10], the work pushed toward higher finesse cavities and thinner active material [11], all-molecular-beam-epitaxially grown structures [12], and waveguiding microresonators [13], [14] with submicron lateral dimensions [15] and device densities $>10^7/cm^2$. The addition of dopants and electrical contacts to this kind of structure produced more than one-million low-threshold VCSEL's on a single GaAs chip [2], [16]–[19].

This paper contains four principal sections—design issues, epitaxial growth, fabrication, and performance characteristics—written by the first four coauthors, respectively. We attempt to make it as generally applicable as possible, but we are naturally inclined toward the techniques and devices we have produced. Applications issues have necessarily been left out to maintain reasonable length.

II. Design Issues

A generic VCSEL is shown in Fig. 1. If the active material is a single quantum well (SQW) of GaAs, ~ 100 A/cm^2 or more is required to reach transparency [20], especially in small-area devices. For N wells, or for bulk material of thickness N times 10 nm, the minimum transparency current density is about N times 100 A/cm^2. Acceptable threshold current densities (<1 kA/cm^2) thus imply an active region of thickness less than ~100 nm. In GaAs lasers, one period of the standing wave field is ~120 nm, so a 100 nm thick layer would be partly wasted by having portions of it in regions of very low optical intensity. Thus, we have restricted our GaAs VCSEL designs to those having active region thicknesses of about 60 nm or less, or more generally, less than one-quarter wave in the material (Fig. 2). Since the active region is necessarily semiconductor material grown by epitaxial techniques, high-quality p–n junctions are easily produced in the *vertical* orientation, while they are very difficult to obtain horizontally [21], [22]. Thus, a thin active layer, narrow p-i-n structure facilitates a low-resistance active region having low current density requirements.

Manuscript received November 14, 1990; revised February 26, 1991.

J. L. Jewell and Y. H. Lee are with AT&T Bell Laboratories, Holmdel, NJ 07733.

J. P. Harbison, A. Scherer, and L. T. Florez are with Bellcore, Red Bank, NJ 07701.

IEEE Log Number 9100201.

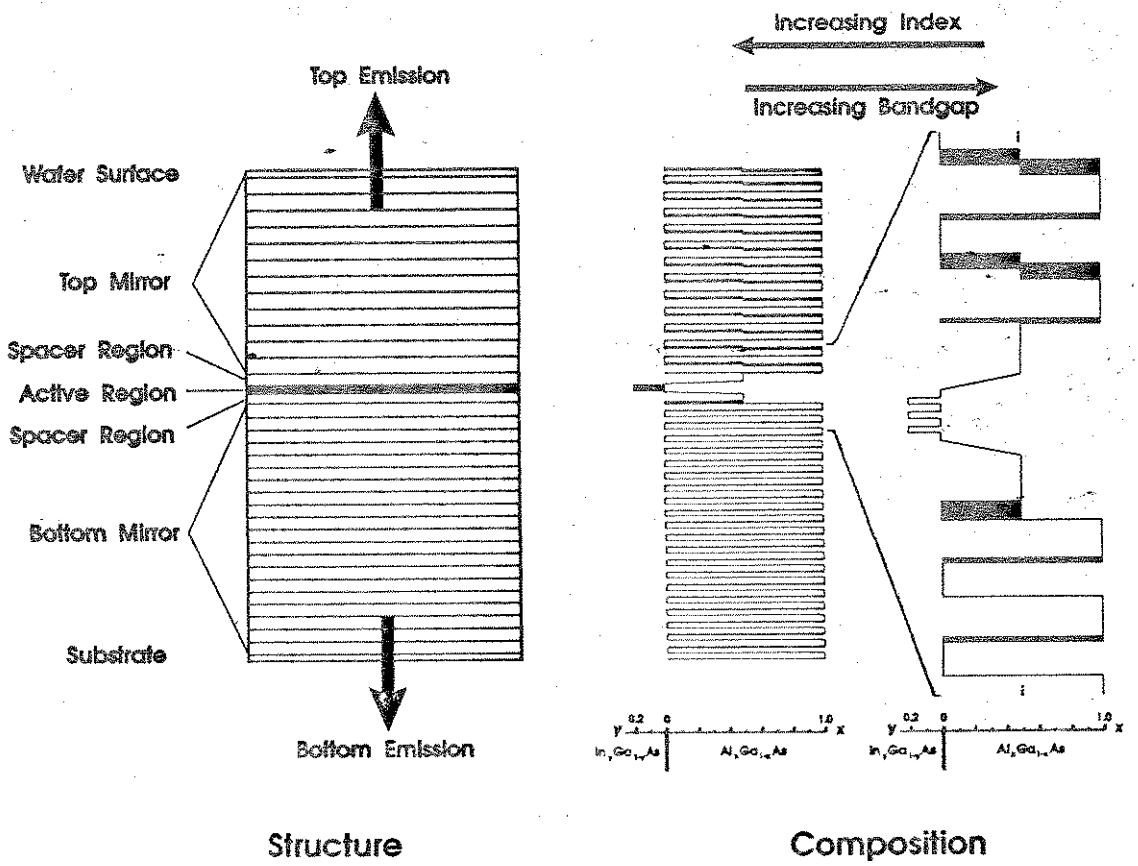

Fig. 1. Schematic representation of a vertical-cavity surface-emitting laser, shown on the left, together with the compositional layer structure used in an actual device shown in the middle, and, in more detail, around the central active region on the right. Solid regions in the compositional structure indicate sections of rapidly alternating layers, inserted to assist current flow across otherwise abrupt heterojunctions.

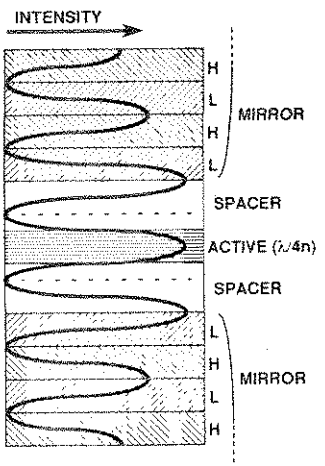

Fig. 2. Standing wave intensity distribution in the central region of a VCSEL. The active region thickness shown is one-quarter of the operating wavelength λ, divided by the refractive index n. H and L denote high and low index layers, respectively, of the mirror.

Since the gain per pass of such an active region is on the order of 1% [20], mirror reflectivities greater than 99% are required. So far, the lowest threshold VCSEL's employed a single quantum well (SQW) of InGaAs active material [17], [23], [24]. Periodic gain structures [22], [25] can accommodate arbitrarily large thickness by placing active layers in the high-intensity lobes, but a rather long cavity results in which longitudinal current flow would generally encounter high resistivity. Top-surface emitting lasers [25], [27]–[30] emit light through a window in the top electrode, and have exhibited the highest room-temperature CW powers to date.

The mechanism desired for achieving confinement of the electrical current and optical field depends on the laser's transverse dimension. VCSEL's of diameter 10 μm or more are desirable when ultralow threshold is not required; gain guiding is sufficient and has been achieved by ion implantation [26]–[31]. This has the attractive feature of preserving planarity in the wafer. Submicron diameters, on the other hand, require strong optical waveguiding such as that obtained by etching vertically throughout the optical resonator. Otherwise, diffraction losses are too high to allow lasing. Such devices may find uses in optical switching or interchip communication where high speed and low power are absolutely necessary. Their performance may be further enhanced by the microcavity's effect on the spontaneous emission. For diameters ~3–10 μm, a combination of gain guiding and waveguiding can be used in a continuously variable fashion which corresponds well with calculations of diffraction loss [18].

Maximum power obtainable from a single device depends largely on the cooling capability and the power efficiency P_{eff}. The latter can be expressed in terms of the

differential quantum efficiency η_{eff}, threshold current I_{th}, operating current I_{op}, lasing photon "voltage" V_g (basically the bandgap energy in eV, normalized by the electron charge), and series resistance R, as

$$P_{\text{eff}} = \eta_{\text{eff}} \cdot \frac{(I_{op} - I_{th})}{I_{op}} \cdot \frac{V_g}{(V_g + I_{op}R)} \qquad (1)$$

assuming the classical L-I curve with zero output at threshold and a constant slope, η_{eff}, above threshold. The product of all three numerators is the output power. The second factor of (1) illustrates the necessity of operating far above threshold for power efficiency. The denominator of the third factor is simply the operating voltage drop across the device. It shows explicitly that series resistance is not the sole indicator of electrical efficiency. For example, scaling devices to larger areas decreases R, but the larger currents required can result in a similar voltage drop and therefore no significant change in efficiency. A more relevant quantity for expressing a diode laser's electrical performance is the voltage required for threshold. Obtaining high P_{eff} in VCSEL's and edge emitters is the same: minimize resistivity and threshold current density, and provide effective heat removal.

Assuming that P_{eff} is sufficiently high so that cooling is achievable, the maximum power is determined by the maximum internal intensity allowable and the maximum cross-sectional area for single-mode operation. Reasonable, but certainly not ultimate, values for these are 10^7 W/cm^2, and 200 μm^2 (16 μm diameter), based on our experiments together with data for commercially available edge emitting lasers. Assuming a 1% transmitting output coupler, this yields about 200 mW maximum power. It is tempting to increase this by using a lower reflectivity output coupler; that, however, implies an increase in the active material thickness. That increased thickness will increase I_{th}, thus increasing current and cooling requirements which may well not be achievable. A more promising approach is to increase the single-mode diameter by increasing the cavity length with nonactive material. Due to light penetration into the mirrors, all-semiconductor AlGaAs-based VCSEL's have a minimum effective cavity length of about 1 μm [32]. Adding 1 μm to this should approximately double the cross-sectional area for single-mode operation and therefore double the maximum power, ignoring effects such as thermal lensing caused by temperature variations across the device. However, adding *doped* material increases the cavity loss, which decreases efficiency. Using *undoped* material requires transverse current flow and the voltage drop increases, thereby also decreasing efficiency. Thus, this approach may be rather limited as well. Pulsed peak powers as high as 120 mW have been reported from $\sim$35 μm diameter thick cavity VCSEL's with high current densities [33].

Our designs for VCSEL active regions are usually graded-index separate-confinement heterostructure (GRINSCH) structures, very similar to the p-i-n diodes of edge emitters. Thus, the active region resistivities should be comparably low. The excessive resistance in VCSEL's is between the contacts and the active region. Resistance in p-type mirrors is high, largely due to the periodic potential well/barrier structure of the AlGaAs–AlAs. This has been minimized by using nonabrupt interfaces [2], [23], [27]–[30], (34), and/or keeping the maximum difference in Al content to be less than about 60% [34]–[36]. The latter strategy increases light penetration into the mirrors, increasing the round-trip loss in the cavity which can seriously decrease efficiency for very thin active regions. For n-type mirrors, the resistance is somewhat less than for optimized GaAs–AlAs p-type mirrors, and is believed to be caused mostly by the poor conductivity of AlAs. Devices of diameter $\geq$5 μm can employ current spreading in either or both mirrors to decrease R. Use of all these techniques still has not produced VCSEL's with threshold voltages V_{th} much lower than 3.5 V. The lowest reported V_{th} in a VCSEL is 1.8 V, achieved by using silver as the only reflector for the p-side [37]. The Ag–AlGaAs reflectivity of only $\sim$95% implied a thick active layer, thus high current density, and also low overall efficiency. Presently, the approach offering the most hope for power efficient VCSEL's has current flow transversely through highly conductive layers just above and below the active region, and vertically through the junction. As a final point of the resistance issue, conventional designs for very small lasers (of any sort) will produce very high resistance. Efficient edge emitters can have R = 2–5 Ω over areas about 500–200 μm^2. Scaling them down to 1 μm^2 would lead to $R \sim 1$ kΩ.

Ultralow threshold ($<$100 μA) in diode lasers implies very small volume of active material. VCSEL's are very straightforwardly scalable to volumes on the order of 0.002 μm^3 (SQW in a 1/2 μm diameter), but fabrication becomes quite challenging. Surface recombination is a serious problem for small-diameter GaAs VCSEL's, and steps are being taken to reduce or eliminate it [38], [39]. For InGaAs devices at 1.3–1.55 μm, the recombination velocity is about 100 times less [40]. GaAs–AlAs waveguides $\lesssim$1 μm in diameter also exhibit waveguide dispersion which shift the cavity resonant wavelength by $\sim$50 nm at 0.5 μm diameter [15]. This means that devices in this size range must first be designed with thicker layers to compensate for the shift, then fabricated with strict tolerances on the diameter. The reward for such fabrication may be much more than simply a smaller volume. The spontaneous emission factor of the fundamental mode (SEF, which is the fraction of spontaneously emitted photons which couple into the laser cavity's fundamental mode) can approach unity for such devices, compared to SEF's of 10^{-4}–10^{-5} in conventional lasers [41]. Microcavities can even enhance the rate of spontaneous emission into the lasing mode, while suppressing emission in other directions [42], [43]. This could lead to extremely fast, efficient devices with thresholds on the order of 10 nA. Nontraditional current injection schemes such as real

space transfer [44] may offer fast, efficient means for driving such devices.

It is advantageous from many standpoints to have the entire VCSEL structure (except for electrical contacts) be a single crystal grown by techniques such as molecular beam epitaxy (MBE) or metal-organic chemical vapor deposition (MOCVD). Mechanical and optical quality are very high, thermal conductivity is good, and the number of fabrication steps is minimized. The materials available for this kind of structure are severely restricted, however, and are generally limited to semiconductors whose lattice constants do not vary greatly, and whose chemical properties are compatible. For GaAs VCSEL's, the obvious choice for mirrors is AlAs–AlGaAs quarter-wave stacks. Since these materials have refractive indexes about 3.0/3.5, it takes 20–30 periods to produce 99.9% reflectivity, and VCSEL structures are typically 5–6 μm thick. This takes a full day's growth by MBE. Furthermore, the thickness accuracy is about $\pm 1\%$, assuming a gain bandwidth about 1% of the optical frequency and a short cavity. This accuracy is about the limit of current state-of-the-art MBE systems. For 1.55 μm VCSEL's, the situation is much worse. "Convenient" materials (in this case, not containing Sb) available have a refractive index difference only ~ 0.2–0.3, so about twice as many pairs are needed as for AlAs–AlGaAs [45], [46]. Each layer must also be about twice as thick so the total VCSEL thickness would be > 20 μm. Alternatively, one or both mirrors can be dielectrics. Fabrication becomes more complicated, but layers of widely differing refractive indexes, e.g., SiO_2–Si [47], [48], can be used to make shorter faster cavities in which spontaneous emission properties may even be enhanced [49]. Use of *in situ* optical monitoring during dielectric film deposition routinely produces thickness accuracies much less than 1%. Practical VCSEL's at 1.3–1.55 μm will very probably have dielectric mirrors; at shorter wavelengths, the tradeoffs are more even. If at least one of the mirrors is epitaxial, a tremendous advantage for processing is gained by not having to remove the substrate.

III. Growth

One unique feature of these latest vertical-cavity structures is that both the central light-emitting GRINSCH region and the outermost Bragg reflectors which define the Fabry–Perot cavity are all dimensionally defined in one integrated crystal growth sequence performed over the entire wafer using molecular beam epitaxy (MBE). The details of one such typical structure are shown in Fig. 1, illustrating the use of carefully controlled layer structures achieved by MBE in the formation of many of the key elements in the device including the active layer quantum wells, graded confinement barriers, spacer layers, alternating index Bragg reflectors, and graded short period superlattice structures between mirror layers to promote carrier transport. The high lateral thickness uniformity achievable in a modern MBE growth system ensures that if the design parameters are properly met at one point on the wafer, they will carry over to within about 1% uniformity across the entire wafer employing substrate rotation to achieve this high level of uniformity. This leads to extremely high yields (in excess of 99%) and, perhaps even more importantly, high uniformity in individual device characteristics across large two-dimensional arrays, which is of vital importance in most array applications.

Achieving this high degree of precision places severe demands on the MBE growth process. The realization of the proper emission wavelength from the central $In_yGa_{1-y}As$ quantum wells through growing the proper quantum well thickness and indium concentration, y, is demanding, but no more so than in an edge-emitting laser which must be properly grown to operate at a specific wavelength. What makes the growth task so much more difficult in the case of an integrated semiconductor-mirror vertical-cavity structure is the extremely tight demands on the layer thicknesses of the mirror layers. As discussed in the previous section, because the length within the cavity over which gain is achieved is so much shorter for a vertical-cavity design than it is for an edge emitter, the mirrors need to be of exceedingly high reflectivity, typically in excess of 99%. Since the partial reflection at each AlAs–GaAs interface in the Bragg reflector is only about 0.6%, many such interfaces need to be stacked together in order to achieve the desired high overall stack reflectivity. In order to achieve this high reflectivity, each repeated layer in the stack must be nearly the same as the others in order to get the proper constructive interference between all the layers. This high degree of periodicity, however, is relatively straightforward to obtain in an epitaxial growth technique such as MBE through the use of precise repetitive shutter timing from period to period, as long as sufficient attention has been given to keeping the effusion cell source stability and hence growth rate stability under tight control for the relatively long periods of 8–12 h required to grow these structures.

The cavity resonances for these high-finesse Fabry–Perot cavities are very narrow, typically $\leq 0.01\%$ of the optical frequency, essentially a delta-function for our purposes here. The requirement that the spectral position of this resonance fall within the relatively narrow 1% wide gain region of the active quantum wells places a severe constraint on the optical thicknesses of the layers making up the cavity. Not only does this requirement demand an exact knowledge of the alloy concentration, since the optical index is composition dependent, even more stringently, it demands *absolute* growth rate control to within 1%. Only by knowledge and control of the semiconductor growth rate determined for each of the group III components to within this 1% tolerance is it possible to meet these stringent requirements. The remainder of this section of the paper will discuss in detail how MBE has been used to achieve this necessary high level of control. Although for clarity we will concentrate on the 980 nm strained InGaAs quantum well structures, most of the specific issues discussed apply equally well to other similar

designs, including the 850 nm GaAs quantum well devices which are also included later in the characterization section of this paper.

The MBE growth system we have used is a Varian GEN II configured to accept 2-in diameter indium-bonded GaAs substrates. The eight effusion cells employed consist of 1) four upward-looking 16 cc cells for the group III elements (In, Ga, and two Al) designed by Varian with trumpet-shaped crucibles for high uniformity across the entire substrate; 2) two cells (also the 16 cc design, prepared for downward-looking operation as previously described by Collins [50] containing the n- and p-type dopants, Si and Be; 3) one 40 cc downward-looking As_4 cell employing a seven-hole boron nitride end cap; and 4) a downward-looking two-zone Varian cracker cell for supplying As_2. Surface emitting laser structures have been grown using each of the two alternative arsenic sources, As_4 and As_2, with no systematic differences in the resulting devices. One modification made to the system to eliminate the rather large flux transients recorded using the beam flux ionization gage when the group III sources were opened was the addition of double-sided 4.5-in conflat flanges on each of the 16 cc cell ports to bring them back away from the shutters, thus minimizing the closed-shutter overheating known to cause the transient effect. This was found to drop the transient, which has a time constant of approximately 1 min, from the 20% range down to a reasonably small and reproducible value of 4%.

The most important part of the process used to achieve the 1% thickness control discussed earlier is the careful monitoring of oscillations in the intensity of the specularly reflected spot of the reflection high energy electron diffraction (RHEED) pattern. Neave *et al.* [51], as well as others, have shown quite elegantly how each oscillation corresponds to precisely one monolayer of deposition. By carefully measuring this period, the exact growth rate can be determined. The data acquisition system we employ involves an optical fiber butted up to the portion of the RHEED screen containing the specular spot, coupled on the other end to a photomultiplier tube. The amplified current output of the photomultiplier is digitized approximately 20 times/s and fed through a CAMAC interface into a micro-PDP 11 computer where it is analyzed in software. After a five-point smoothing routine is performed on the data, the maxima and minima are determined and a section of adjacent periods, usually numbers 2–12, are measured, and a resulting rate is calculated, taking into account the 4% flux transient correction discussed above.

One key issue in getting reliable 1% control of rates comes in the reevaporation of the more volatile group III species during growth above a certain critical temperature (In in the case of InGaAs and Ga in the case of AlGaAs). Although, in principle, RHEED oscillations measure not just the group III arrival rate but the actual growth rate consisting of that arrival rate *less* the reevaporation rate, this reevaporation rate is strongly substrate temperature dependent. Since the RHEED oscillation calibrations are performed *prior* to the actual growth on a small test sample centrally mounted on a *different* Mo sample block, any differences in the actual surface temperature, a quantity which is in general very difficult to measure accurately, will result in *different* reevaporation rates for the RHEED test sample and the actual wafer. The differences become more pronounced at higher substrate temperatures. It is for this reason that we have chosen in these structures the requirement of such a high degree of precision to remain in the substrate temperature regime where such reevaporation effects are negligible on the scale of 1%. This means growing the GaAs–AlGaAs–AlAs layers at 580°C and the InGaAs at 530°C, determined by substrate thermocouple readings calibrated for each run to the known oxide desorption temperature of 580°C. Admittedly, this is a compromise, trading off optimal crystal quality attainable at higher substrate temperatures against higher rate control attainable at lower temperatures. As better forms of substrate temperature measurement become available, this compromise will become less severe.

Staying in the negligible group III reevaporation regime has the added advantage that the requirements of exact timing of substrate temperature changes and the need to return to precisely the same substrate temperatures are made much less stringent. This is not true, however, of cell temperatures, as will be discussed below. The use of relatively thin AlGaAs ternary alloy layers, coupled with the frequent use of short period superlattices, helps avoid rough interface problems resulting from low substrate temperatures, which is highly undesirable in high-reflectivity structures such as these. These issues become more severe in shorter wavelength VCSEL structures employing GaAs (rather than InGaAs) active layer quantum wells, because in such structures the dielectric stacks become AlAs–AlGaAs rather than AlAs–GaAs, exacerbating this smooth growth problem [52].

Using the above methodology, the rates of each of the Ga and Al cells is measured at least three times, allowing at least 2 min between each measurement for the 4% flux transient to be reproducibly reestablished. If the three values do not lie within a few percent of each other, the measurements are repeated. For the case of InAs, which severely lattice mismatched with the GaAs RHEED sample and hence will not grow pseudomorphically long enough to get a sufficient number of RHEED oscillations, the rate of InGaAs is measured directly by observing oscillations on simultaneously opening the In and Ga shutters. Once all the rates have been measured in the manner just described, small adjustments are calculated for the cell setpoints based on previously determined Arrhenius plots for each cell, and the cell temperature adjustments are made. After equilibration times of at least 15 min for the cells to adjust, the measurement process is repeated. This entire cycle is repeated as many times as necessary to arrive at calibrated growth rates within the 1% tolerance required.

Some final comments are in order on three important requirements for the growth of these structures. The first

two requirements—shutter reliability and thickness uniformity across the entire wafer—are a function of the particular MBE system used. They are both primary concerns of the MBE manufacturers when they design their systems, but it is worth pointing out that the demands imposed by the surface emitting laser structures discussed here (1% uniformity and up to 1000 shutter operations *per wafer*) are severely pressing those manufacturer's designs to the limit, and can only be attained in an optimized state-of-the-art MBE growth system. The third requirement, that of cell flux stability, has components tied both to the manufacturer and the user. The requirement that the RHEED determined rate, determined at the beginning of the day, hold constant to within 1% over the remaining 8–12 h of the subsequent growth run is a rather stringent design specification to put on a cell/temperature controller combination, but our favorable results in growing these structures indicate that this design need has in fact been met by the manufacturer. What we have done as a user to further ensure this constancy is to hold the cells at constant temperatures *throughout* the growth run once the RHEED calibrations have been performed. Changing a cell temperature in the middle of a run to achieve a different alloy concentration, and then changing it back to continue at the nominal starting rate, does work to within a few percent, absolute, but is most likely a risky business in achieving the desired 1% reproducibility. It is for this reason that when growing these structures we calibrate at the beginning of *each* day (the cells are idled a few hundred degrees cooler overnight) and hold the cell temperatures constant thereafter. Extra combinations of alloy concentrations are then achieved by the use of multiple cells (two Al cells in our case) and by the use of short period superlattice chopping to achieve different average concentrations. It is also by means of this latter technique that any graded regions are introduced into the sample. In this way, the necessary high precision required in these structures can be achieved and maintained.

IV. Fabrication of Vertical-Cavity Surface-Emitting Lasers

Vertical cavity devices, such as microlasers, are ideally suited for integration into large numbers of nearly identical low-threshold array elements. Through the application of lithographic techniques and ion processing, the diameters of individual microlasers have been reduced to below 1 μm. The accompanying reduction in active volume can be used to further decrease the threshold currents required to operate these microlasers, and permits us to combine them into more complex, coherently coupled arrays. In this section, we describe the techniques which we have employed so far to fabricate surface-emitting microlasers; these currently involve ion etching and/or ion implantation. We also describe methods of packaging these devices into large arrays, and discuss the limitations to their further miniaturization and threshold reduction imposed by our present fabrication tools.

A. Microlaser Geometries

Conceptually, the simplest method of defining a vertical-cavity device from a grown wafer relies on the physical removal of the material everywhere except for the cavity itself. This is typically accomplished by masking the shape of the laser, and etching away the unwanted semiconductor by using either a suitable chemical solution of a reactive ion process [19]. We thereby transfer the laser shape through the grown layers. A schematic of the resulting "vertical waveguide" is shown in Fig. 3(b). The original MBE-grown laser material consists of a stack of layers with large compositional changes, and nonselective chemical "mesa" etching can only be applied to structures with widths above 20 μm. Microfabrication of smaller waveguided lasers thus relies on ion-assisted processes, such as reactive ion etching (RIE) or chemically assisted ion beam etching (CAIBE). With these anisotropic etching techniques, the sizes of electrically pumped lasers have been reduced to 1.5 μm in diameter [Fig. 3(a)] [2]. This vertical waveguide geometry results in a large surface-to-volume ratio and substantial sidewall ion damage produced by exposing the sidewalls of such structures to the ion beam and to sidewall oxidation [53]. Another major problem of this design lies in the poor heat sinking of the laser cavity. Therefore, in pulsed operation, we typically observe increased threshold current density in devices below 10 μm in diameter, whereas the total threshold current increases below 3 μm. However, in spite of these limitations, threshold currents as low as 0.8 mA have been measured on chemically treated vertical waveguide microlasers [2].

We have also isolated lasers by only defining the top mirrors and the lasing cavity [Fig. 4(a)] [18]. This requires only half the etch depth, results in better heat sinking of the laser cavity, and leads to improved CW laser performance. However, diffraction losses prevent us from arbitrarily decreasing the sizes of active devices much below 5 μm. Since, in this structure, the Si-doped mirrors are still intact and can be used as the bottom contact, this structure is particularly applicable to integrating microlasers into matrix-addressable arrays. Alternatively, we can use ion implantation to selectively shut off electrical conductivity in the p-doped top mirror, thereby producing the gain-guided structure shown in Fig. 5(a) [26]–[31]. This is accomplished by proton bombardment or ion implantation of heavier species. The ion damage provides a "cloud" of disrupted material underneath the mask, which limits the resolution of the pattern transfer. Again, diffraction losses limit the ultimate size of structures. However, since the sidewalls of the quantum wells are not exposed to atmosphere in this geometry, surface recombination and cavity heating are reduced, resulting in better CW performance [28]. There are also processing advantages to retaining the surface planarity using the ion implantation process, especially for complex fabrication schemes involving large arrays. Finally, combinations of ion etching and ion implantation have also been employed

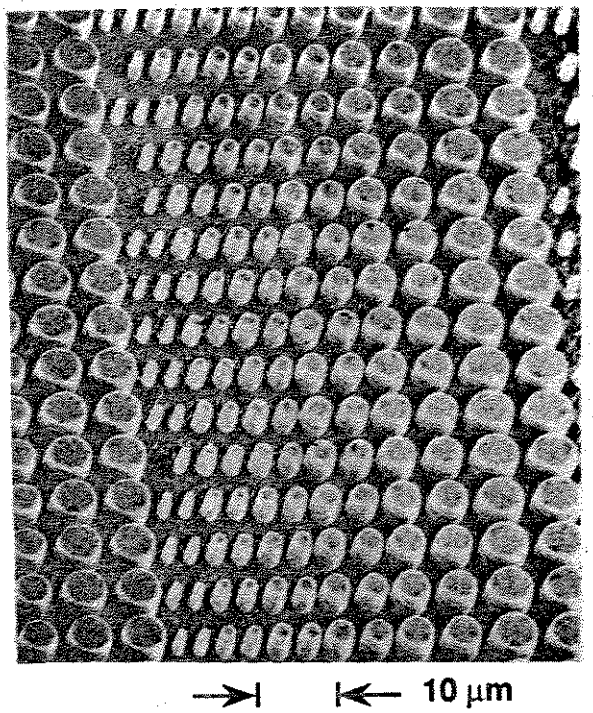

Fig. 3. (a) and (b) SEM micrograph and corresponding schematic of ion beam etched microlasers with diameters ranging from 1 to 5 μm.

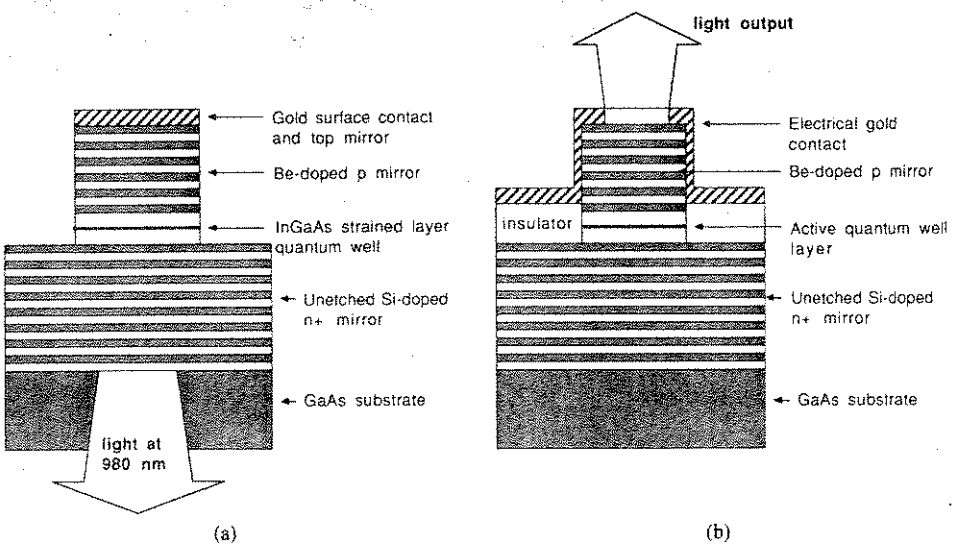

Fig. 4. (a) and (b) Schematics of front and back emitting microlasers defined by etching through the active region.

to avoid surface recombination and still limit the diffraction losses from small lasers [18]

B. Ion Implantation and Masks

Ion implantation has been used to produce implantation damage to define a limited conducting region in the active p–n junction. The depth of the implantation depends on the ion mass and energy. In order to selectively implant H^+ to a depth of 2.5 μm in AlGaAs, ion energies of 300 keV at a dose of 2.5×10^{14} cm^{-2} are required [26]–[30]. To protect the conducting active laser region during this implantation, approximately 6 μm of photoresist mask is required. This thick layer of photoresist is generally defined with a tri-level resist scheme, which has also been used to lift off a self-aligned p-type Au–Zn contact [30]. These top surface-emitting lasers, schematically drawn in Fig. 5(b), are then annealed both to alloy in the contact and to anneal the slight damage in the upper layers, thus reducing the surface resistance. The key to processing these ion-implanted lasers lies in the fabrication of an appropriate implantation mask, and choosing the correct implantation species.

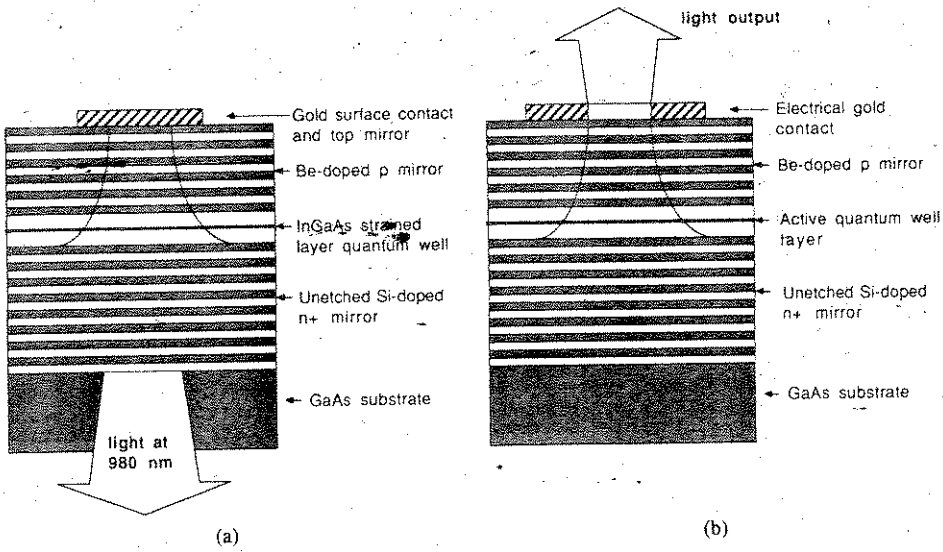

Fig. 5. (a) and (b) Schematics of front and back surface-emitting microlasers defined by ion implantation and gain guiding.

Masks used for ion etching and ion implantation have to satisfy fundamentally different requirements. Ion etch masks require good chemical stability of the mask material in the reactive etch chamber atmosphere, resulting in a good "selectivity" of the semiconductor material etching rate over the mask erosion rate. Ion implantation masks, on the other hand, should provide a large cross section to high-energy ions bombarding the material, and are typically much thicker. Metal masks are preferred for both cases, and can be used in structures where light is emitted out the substrate and through the back of the wafer [2], [16]–[19], [23], [24]. Nickel and chromium are particularly good CAIBE masks [54], whereas gold and tungsten are generally used for ion implantation. If laser emission is required from the surface of the wafer [Fig. 4(b) or 5(b)], removable masks have to be used with multilevel lithography. For ion implantation, such a mask stack can consist of 0.3 μm of SiO_2, 6 μm of hard-baked (200°C, 1 h) photoresist, 0.1 μm of evaporated Cr, and thin positive photoresist. In this fabrication scheme, the Cr layer is defined by wet etching using the top photoresist mask, and then this pattern is transferred by reactive oxygen etching through the 6 μm implantation mask. The SiO_2 layer is then removed in the contact area, the sample is implanted, and p-type contacts are evaporated. Finally, the hard-baked photoresist mask is stripped with photoresist stripper, simultaneously lifting off the contact metal [27]–[30]. Alternative single-level inorganic mask materials, such as silicon dioxide, silicon nitride, or tungsten, have also been employed to microfabricate lasers, and can subsequently be removed in a freon–oxygen dc plasma discharge.

C. Ion Beam Etching

GaAs–AlAs multilayers can be etched both by RIE and CAIBE with aspect ratios in excess of 10:1. To define VCSEL's, 3–7 μm of this DBR mirror material must be nonselectively removed. In general, chlorine-based reactive gases are ideally suited for such nonselective etching GaAs and AlAs layers [13]. The most important practical consideration during this etching process is to avoid buildup of aluminum oxide on the Al-containing layers, which reduces the etch rate and roughens the sidewalls of the etched microlasers. BCl_3 mixtures are therefore often used to avoid oxide buildup during RIE [55], [56]. Another approach lies in increasing the etch rates, which also increases the etch rate selectivity of the AlAs–GaAs over the mask materials. We find that the high etch rates and anisotropy of CAIBE [57] makes it ideal for microfabricating of vertical-cavity optical devices. In our system, a Kaufman ion source is used to generate ion beams of Xe^+ with energies between 500 and 1000 eV. The inert gas flow is regulated with a mass flow controller to 4.5 sccm for Xe, and the sample surface is exposed to a Cl_2 flux of approximately 10 sccm which locally increases the sputter yield.

For any combination of ion energy, flux, and sample surface temperature, the partial pressure of reactive gas (p_{Cl_2}) must be optimized for maximum anisotropy and etch rate [19]. Generally, if (p_{Cl_2}) is too low, angled sidewalls result and trenches are formed next to the etched microstructures. Conversely, when (p_{Cl_2}) is too high, undercutting of the mask is evident. If the etching process is interrupted, a step results in the sidewall profile. Such a step is attributed to the oxidation of AlAs mirror layers forming Al_2O_3, which then acts as an ion etch mask.

High etch rates are needed to etch deep features, such as the 5.5 μm microlaser structures, and still retain the necessary vertical sidewall profile. In CAIBE, fast and nonselective etching can be obtained by increasing the ion energies above 500 eV. However, at such high ion energies, ion damage can introduce recombination and scattering centers close to the etched vertical sidewalls [58], [59]. To microfabricate low-threshold lasers on the <5 μm scale, we therefore not only need to control the sidewall smoothness and the anisotropy of the microfabri-

cated structures, but we also have to minimize the extent of the ion-induced damage to the structure sidewalls. In CAIBE systems, a decrease in the ion energies reduces such damage, but also causes a deterioration of the anisotropy. Instead, we have selected a heavy ion milling species, Xe^+, which, with a lower velocity, reduces the ion damage while still producing the required etch rate and anisotropy [19].

D. Packaging into Arrays

The MBE-grown laser material and the laser definition techniques described in the previous subsections allow us to produce many nearly identical laser elements. This attribute of microlasers was used to package these devices into individually addressable arrays. These fall into two categories: 1) independently addressable arrays in which a separate contact made to each array member, and 2) matrix-addressable arrays in which contacts are made to columns and rows only. Ion implantation is fundamentally planar, facilitating the metallization steps needed to provide electrical contact to the lasers. When ion beam etching is used, material surrounding each laser is removed, necessitating replanarization. To date, both independently addressable [60], [61] and matrix-addressable [62], [63] arrays, using the proton implantation process for the laser definition, have been successfully designed, fabricated, and tested. Fig. 6 shows a top view of an 8 × 8 independently addressable VCSEL array. The top portion of Fig. 7 shows schematically how the matrix-addressing scheme is incorporated into the VCSEL wafer. The fabrication of this particular array requires a combination of *both* ion implantation *and* etching techniques. The bottom of Fig. 7 shows a top view of a 32 × 32 array formed in such a manner. This matrix-addressable array contains 20-μm diameter VCSEL's, fabricated on a 100 μm pitch. Including the bond pads at the perimeter, this 1024-laser array occupies ~4 mm × 4 mm of wafer area.

In Fig. 8, we schematically describe the processing steps involved in fabricating a matrix-addressable array of surface-emitting lasers when ion etching is chosen as the definition step. First, the individual laser elements are defined by etching through the active layer, using photoresist as an etch mask. Then, trenches are etched to define the bottom (n-type) contact, again using photoresist as an etch mask. Polyimide is spun onto this structure to fill these trenches, and provide an insulating layer between the n and p contacts. SEM micrographs of a matrix-addressable array after oxygen plasma etching of the polyimide to expose the upper laser contact is shown in Fig. 9(a). Following this procedure, the laser definition mask is again used to cover the top contacts with photoresist. Then, gold is angle evaporated to establish the p contact, and lifted off from the laser tops. The last lithography step involves ion milling of the gold into stripes to define the top contact bars followed by oxygen RIE etching to expose the bottom contacts. The completed matrix-addressable device is shown in Fig. 9(b), where 1024

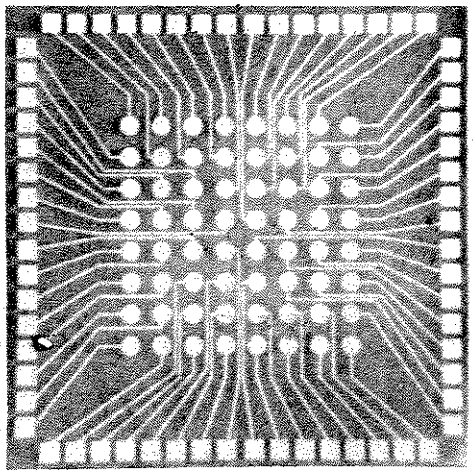

Fig. 6. Top view of an 8 × 8 independently addressable vertical-cavity surface-emitting laser array fabricated by ion implantation techniques. The lasers, 20 μm in diameter, are in the center of the large circular contact pads.

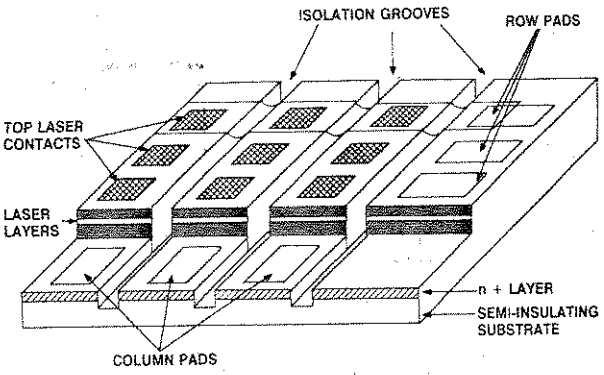

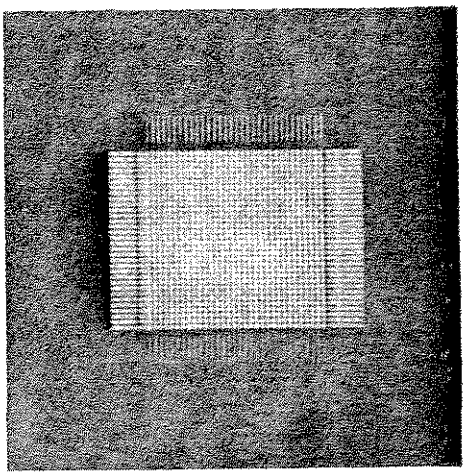

Fig. 7. Upper half shows the schematic of a matrix-addressable vertical-cavity surface-emitting laser array requiring a combination of etching and ion implantation techniques. The lower portion is a top view of such a matrix-addressable 32 × 32 surface-emitting laser array. Lasers are 20 μm in diameter, separated by 100 μm. Bond pads around the perimeter provide for contact to the n/p (rows/columns) side of the devices.

20 μm wide elements are separated by 50 μm center-to-center spacing and fit into a 2.3 mm × 2.3 mm area. A simpler air-bridging procedure has allowed us to define an 8 × 8 matrix of independently addressable lasers,

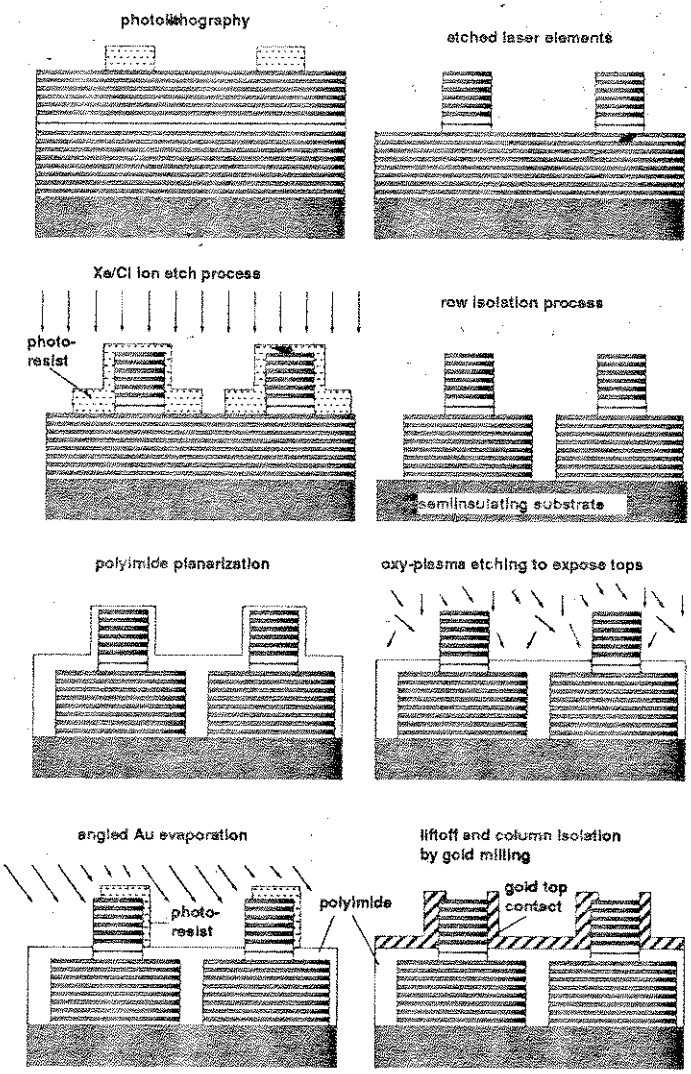

Fig. 8. One of the processing sequences employed to define a matrix-addressable microlaser array by ion etching.

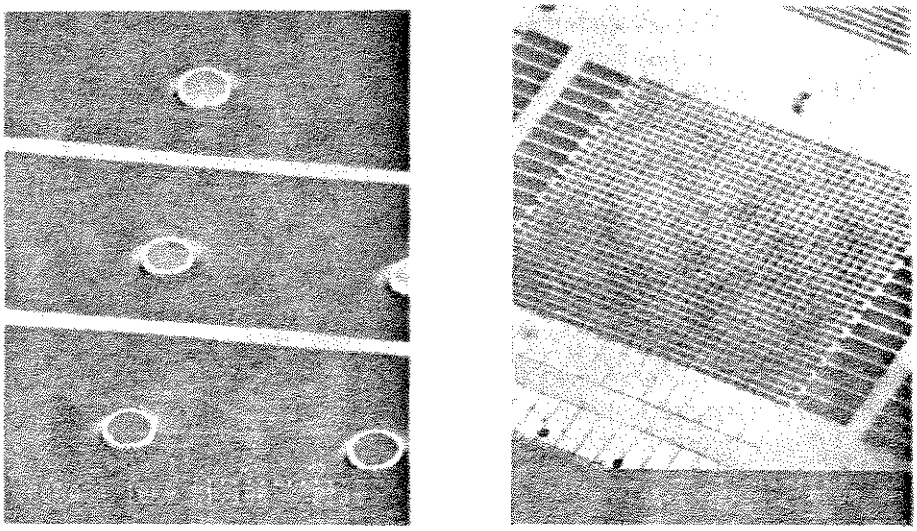

(a) (b)

Fig. 9. (a) and (b) SEM images of 32 × 32 matrix-addressable laser array after polyimide planarization and after complete processing.

which in this case only share the bottom (n-type) contact, and require individual p contacts.

E. Ultrasmall Devices

Threshold currents of vertical cavity microlasers are dominated by the active volume and the surface recombination of carriers at traps formed by ion damage or surface oxidation. A wet chemical treatment [39] of the surface of a 5 μm laser after ion etching was used to reduce the threshold current from 1.5 mA to 0.8 mA (Fig. 10). Even without surface passivation treatments, optically pumped SQW lasers have been fabricated to sizes of about 0.5 μm in diameter. During the fabrication of these submicron laser structures, vertical, 7 μm long waveguides have to be defined to confine the pumped light inside the mirror structure. The resulting lasers have aspect ratios of as high as 15 : 1, and are shown in Fig. 11. Electron beam lithography is typically used to define the masks used for the definition of such ultrasmall lasers, and high-resolution optically transparent etch masks, such as $AlSrF_2$ [64] are used to define the individual elements.

Heating of the laser structures during the ion beam etching process is one of the many problems we encounter when defining such highly anisotropic devices. Although the substrate is heat sunk, these small structures can no longer be conductively cooled during the fabrication or during the measurement process. It is therefore critical that the sidewalls of such structures are exposed to the reactive gas for a minimal amount of time, and spontaneous chlorine etching of the semiconductor material is controlled. This is accomplished by etching at very high material erosion rates, or by cooling the substrate. If it is possible, through such passivation or regrowth techniques, to decrease the surface recombination rate of such structures, the sizes of individual laser elements can be further reduced by electron beam lithography [64], and very low threshold currents can be achieved.

V. Characterization

In this section, characteristics of surface-emitting lasers with few quantum wells are exclusively summarized and compared. They are 980 nm InGaAs surface-emitting lasers (three quantum wells and a single quantum well) and 850 nm GaAs (four quantum wells) top-surface-emitting lasers. Thresholds for the lasers under study are mostly on the order of 1 mA. All experimental data shown here are obtained at room temperature.

The first InGaAs three quantum well (InGaAs 3QW) lasers [16] have bottom (output) mirrors with 20.5 pairs GaAs–AlAs quarter-wave stack and hybrid top (back) mirrors with 12 pairs GaAs–AlAs quarter-wave stack capped by Au film. In pulsed operation, threshold for the InGaAs 3QW laser is ~1.3 mA from a 3-μm diameter deep-etched mesa as shown in Fig. 12. "Deep etched" is defined as when the etch depth is deeper than the bottom mirror such that complete optical guiding is achieved. Room temperature CW operation was observed from a 5-μm diameter 10 nm InGaAs SQW laser etched to just below the active region [17] with 1.5 mA threshold. Chemical passivation decreased it to 1 mA. In both cases,

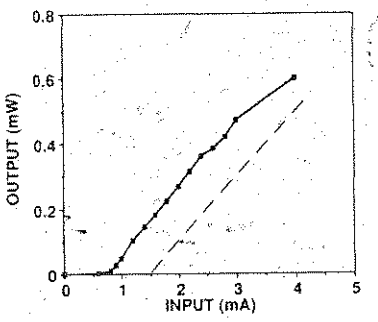

Fig. 10. Pulsed light versus current curve of a 5 μm wide microlaser before (dashed) and after (solid) passivation.

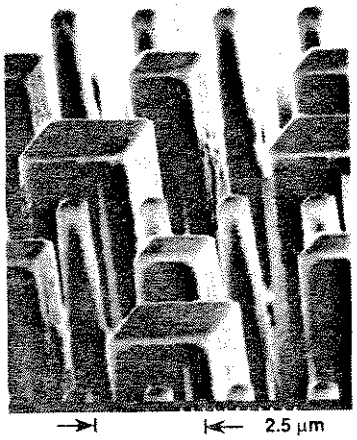

Fig. 11. SEM image of ultrasmall microlasers with widths down to 0.25 μm defined by ion beam etching.

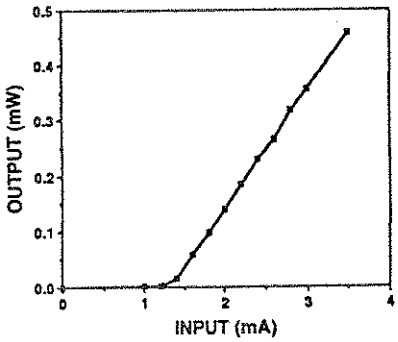

Fig. 12. Pulsed output light versus current in a 3-μm diameter InGaAs 3QW laser.

the output power was limited due to ohmic heating and low differential quantum efficiency. The InGaAs SQW lasers have 23.5 and 15 pairs (plus Au) of bottom and top mirrors to compensate for the reduced gain as compared to the 3QW InGaAs laser. The CW characteristics of InGaAs 3QW structures are later improved [18] by shallow etching just above the active layer and implantation (half gain guiding and half index guiding) to 0.6 mW from a 10-μm diameter laser by improving heat dissipation. Also by implantation isolation [26] of the InGaAs 3QW without etching, fully gain-guided planarized lasers are fabricated with similar performance characteristics. The Santa Barbara group reported the lowest threshold of 0.7 mA from a deep-etched 6 μm square 8 nm InGaAs SQW device [24], at the expense of output power and quantum

efficiency. The laser has 28.5 pairs and 23 pairs (plus Au) of bottom and top mirrors, whose reflectivities are even higher than those of our design. In pulsed operation, peak powers are generally much higher than those of CW cases, indicating nontrivial thermal effects in CW operation. Differential quantum efficiencies are generally 5–30%. The lasing wavelengths are between 940 and 980 nm.

Top-surface-emitting GaAs four quantum well (GaAs 4QW) lasers [27]–[30] have all-MBE structures with 26.5–27.5 pairs of AlGaAs–AlAs quarter-wave layers bottom (back) and 19–20 pairs of AlGaAs–AlAs quarter-wave layers top (output) mirrors designed at 850 nm. Actual lasing wavelengths are 845–850 nm. The characteristic reflectivity spectrum of an as-grown wafer is shown in Fig. 13. Since laser output in this case need not pass through the GaAs substrates, various wavelengths' lasers can be engineered at wavelengths opaque to bulk GaAs (<880 nm) without etching substrates. The deep-proton-implanted [65] GaAs 4QW lasers with current funneling generally have peak CW output powers of >1.5 mW from all sizes tested (10, 15, 20, 30 μm). The maximum CW output power over 3.3 mW [30] was observed from 30-μm-diameter lasers in multitransverse mode operation. The thresholds are 2–10 mA, depending on sizes. Typical optical and electrical characteristics of the lasers are shown in Fig. 14. CW slope efficiency as high as 1 mW/mA was observed for a limited range above threshold, which corresponds to $\sim 70\%$ differential quantum efficiency [29].

Threshold current densities for the InGaAs and GaAs lasers are comparable, ranging from 600 A/cm^2 to a few kA/cm^2, depending on the size of lasers, MBE growth accuracy, material quality, and design parameters. Generally, the operating current density increases with the reduction of sizes, mainly due to nonradiative surface recombination for index-guided structures or diffraction losses and other nonradiative recombinations for gain-guided structures. These values are still much higher than the reported 60 A/cm^2 [66] for *large area* InGaAs edge-emitting lasers. Therefore, there is room for another order of magnitude improvement by proper passivation, wave guiding, and cavity design. Free carrier absorption in the highly Be-doped p-type mirror could be a limiting factor in approaching the cited current density of an edge-emitting laser. One of the main problems of the surface emitting lasers is their high resistance, resulting in high operating voltages. The reason lies in heterointerfacial potential barriers between GaAs (or AlGaAs) and AlAs quarter-wave layers, especially for holes in a p-type mirror as well as poor AlAs conductivity in the n-type mirror. For the InGaAs 3QW laser, graded AlGaAs superlattice layers [2], [23] are introduced between GaAs and AlAs quarter-wave layers in a p-type mirror as schematically shown in Fig. 1. In fact, these barrier-smoothing intermediate AlGaAs layers made possible the operation of deep-etched lasers in pulsed operation with biases ranging between 7–15 V, for 10–3 μm in diameter. Later, shallow etching with 5–10 μm diameters showed improved performance with a bias of 4–6 V, indicating significant resistance in the bottom n-type mirror as well. Lasers laterally defined by proton implantation also operate with bias of approximately 4 V. Generally, dynamic resistances above threshold are a few hundred to thousand ohms for 10-μm diameter devices. All the InGaAs lasers studied by different groups also have AlGaAs graded superlattice to minimize resistances through Be-doped p mirrors.

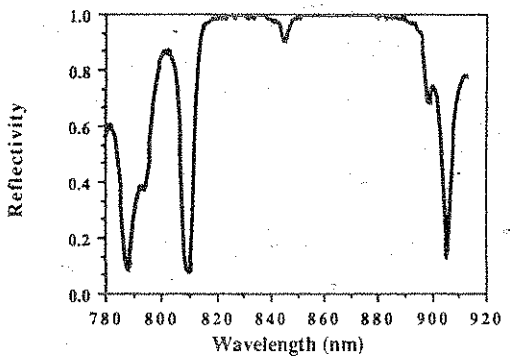

Fig. 13. A typical reflectivity spectrum of an as-grown GaAs 4QW laser wafer.

For the GaAs 4QW lasers, AlGaAs intermediate layers of double step (APA #6) at only one interface [27], [29] and single step (ATT #80) at two interfaces [28], [30] are used in the AlGaAs and AlAs quarter-wave p-type mirror as shown in Fig. 15. Lasers from APA #6 have threshold voltages around 6–17 V, while lasers from ATT #80 have threshold voltages around 4–5 V. Single-step AlGaAs intermediate layers (ATT #80) function comparably to graded AlGaAs superlattices used in InGaAs lasers. The comparison study [34] on resistivities between AlGaAs step and AlGaAs superlattice intermediate layers also reported similar effectiveness. As the size of the gain-guided laser becomes smaller, propagation diffraction losses become more severe with the inverse fourth power of Gaussian beam radius. Therefore, gain-guided lasers much smaller than 5 μm in diameter would be hard to realize, or would be inefficient [3], [18] if possible. But for sizes larger than 10 μm, top-surface-emitting lasers show good room temperature CW characteristics.

Dynamic characteristics were tested for InGaAs 3QW lasers and GaAs 4QW lasers using biased inductance mountings. When connected with a 50 Ω resistor and a chip capacitor, an InGaAs 3QW laser showed 3 dB frequencies of 8 GHz [2]. Gain switching of the same laser using 2 GHz sinusoidal current generates gain-switched pulses with ~ 25 ps full width at half maximum. For GaAs 4QW lasers of 20 μm in diameter, the 3 dB frequency is 3.7 GHz, which is limited by the parasitic capacitance and the 150 Ω differential resistance. The GaAs 4QW laser has an FM response around 3 GHz [67].

Surface-emitting lasers are generally linearly polarized. A detailed treatment of polarization and modal properties of VCSEL's formed by ion implantation can be found elsewhere in this issue [68]. In case of small deep-etched lasers less than 5 μm in diameter, the polarization reflects asymmetry in the etched structure [2], [14]. For implanted (unetched) GaAs 4QW lasers with sizes larger than 10 μm, polarizations are along two cleavage axes of the GaAs crystal. Most lasers start lasing in a Gaussian

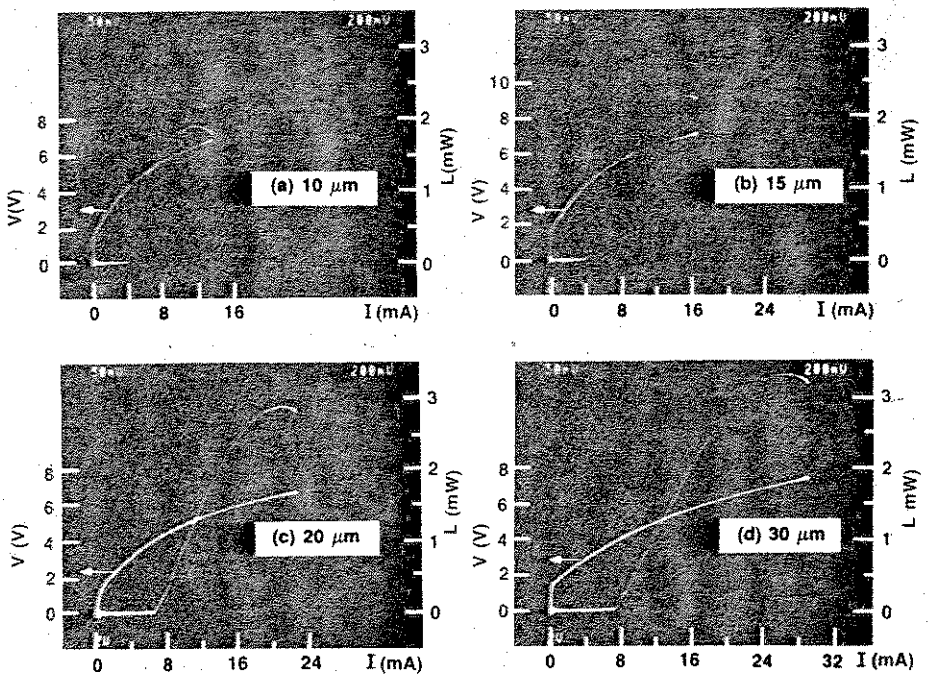

Fig. 14. Room-temperature CW *V-I* and *L-I* curves for adjacent GaAs 4QW lasers of different diameters.

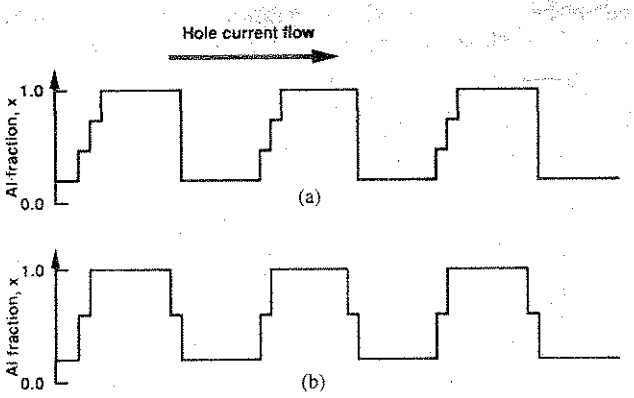

Fig. 15. Two configurations of p-type AlGaAs mirrors implemented for GaAs 4QW lasers. (a) APA #6, and (b) AT&T #80.

mode. When operating gain-guided lasers in a fundamental Gaussian mode, Gaussian beam diameters at $1/e^2$ intensity points are about half of the laser window sizes [29], resulting in twice the divergence of those calculated from a simple diffraction formula using aperture diameters. This seems to be the case for both GaAs 4QW and InGaAs 3QW gain-guided lasers. But high-order transverse modes up to TEM_{22} mode are reported [68] at well above the threshold from 20 μm square gain-guided InGaAs lasers. Only a fundamental Gaussian mode was observed from small (<5 μm square) deep-etched InGaAs lasers. For gain-guided GaAs 4QW lasers (>10 μm diameter), development of higher order modes are observed from all sizes tested. Currently, the maximum CW output power in a fundamental mode is about 0.5 mW. The onset of higher order modes generates noticeable kinks in *L-I* characteristics curves. In principle, the high-order transverse modes are allowed for large lasers. It is not clearly understood, at present, but the onset of the higher order modes could be encouraged by spatially nonuniform ohmic heating leading to slight thermal lensing effects over the laser aperture and/or gain saturation. Laser spectral linewidths are always spectrometer-limited when operating CW in a single transverse mode. For a limited power range <0.06 mW, a linewidth-power product of 5 MHz mW was measured [24] by an interferometric method from an InGaAs SQW laser. Recently, from a 15 μm diameter GaAs 4QW laser running at 0.3 mW CW, a Gaussian-mode spectral linewidth of 50 MHz [69] was measured by optical heterodyne techniques using a commercial single-mode laser diode of 6 MHz linewidth as a reference source. A similar linewidth was measured also from a longer vertical-cavity circular buried heterostructure surface emitting laser [7]. Preliminary data on lifetime testing [70] were collected from only a few GaAs 4QW samples. Laser driving currents were monitored under the constant output power condition (0.8 mW, CW) at 40°C. The data indicate 10 000–20 000 h of lifetime at 20°C, which is still more than an order of magnitude shorter than that of commercial edge-emitting AlGaAs lasers. To be statistically meaningful, additional experimental data should be collected. Even with a high-reflectivity ($>99\%$) output mirror, the peak in-cavity optical intensity of a VCSEL is comparable to that of a typical edge-emitting laser, and the intensity at the laser output facet is much lower in the VCSEL than in the edge-emitting laser, taking the relatively large area of VCSEL's into account. VCSEL's could be as reliable as edge-emitting lasers.

VI. Conclusions

It is expected that VCSEL performances will show significant advances in the next few years. A successful program of development must integrate all aspects including design, crystal growth, fabrication, and testing into one coherent effort. We hope that this presentation of these

aspects in a single paper will aid readers in VCSEL development.

ACKNOWLEDGMENT

The authors would like to acknowledge the contributions of a large group of collaborators without whom this work would not have been possible, including S. L. McCall, B. Tell, K. F. Brown-Goebeler, R. E. Leibenguth, C. A. Burrus, R. S. Tucker, N. A. Olsson, J. M. Van Hove, Y. C. Chung, J. C. Jeong, V. D. Mattera, F. S. Choa, C. J. Sandroff, B. P. Van der Gaag, E. D. Beebe, M. Orenstein, A. C. Von Lehmen, and C. Chang-Hasnain. J. P. H. would like to acknowledge the extensive amount of work done by L. Peterson in setting up the RHEED oscillation measurement system, without which the high degree of precision required for the growth of these structures would have been unachievable.

REFERENCES

[1] H. Soda, K. Iga, C. Kitahara, and Y. Suematsu, "GaInAsP/InP surface emitting injection lasers," *Japan. J. Appl. Phys.*, vol. 18, pp. 2329–2330, Dec. 1979.

[2] J. L. Jewell, Y. H. Lee, A. Scherer, S. L. McCall, N. A. Olsson, J. P. Harbison, and L. T. Florez, "Surface-emitting microlasers for photonic switching and interchip connections," *Opt. Eng.*, vol. 29, pp. 210–214, Mar. 1990.

[3] K. Iga, F. Koyama, and S. Kinoshita, "Surface emitting semiconductor lasers," *IEEE J. Quantum Electron.*, vol. 24, pp. 1845–1855, Sept. 1988.

[4] S. Uchiyama and K. Iga, "Two-dimensional array of GaInAsP/InP surface-emitting lasers," *Electron. Lett.*, vol. 21, pp. 162–164, 1985.

[5] K. Iga, S. Kinoshita, and F. Koyama, "Microcavity GaAlAs/GaAs surface emitting laser with Ith = 6 mA," *Electron. Lett.*, vol. 23, pp. 134–136, Jan. 1987.

[6] F. Koyama, S. Kinoshita, and K. Iga, "Room-temperature continuous wave lasing characteristics of a GaAs vertical cavity surface-emitting laser," *Appl. Phys. Lett.*, vol. 55, pp. 221–223, 1989.

[7] H. Tanobe, F. Koyama, and K. Iga, "Spectral linewidth of AlGaAs/GaAs surface-emitting laser," *Electron. Lett.*, vol. 25, pp. 1444–1446, Oct. 1989.

[8] A. Ibariki, K. Kawashima, K. Furusawa, T. Ishikawa, T. Yamaguchi, and T. Niina, "Buried heterostructure GaAs/AlGaAs distributed Bragg reflector surface emitting laser with very low threshold (5.2 mA) under room temperature CW conditions," *Japan. J. Appl. Phys.*, vol. 28, pp. L667–L668, Apr. 1989.

[9] H. M. Gibbs, S. L. McCall, T. N. C. Venkatesan, A. C. Gossard, and W. Wiegmann, "Optical bistability in semiconductors," *Appl. Phys. Lett.*, vol. 35, pp. 451–453, 1979.

[10] A. Passner, H. M. Gibbs, A. C. Gossard, S. L. McCall, T. N. C. Venkatesan, and W. Wiegmann, "Ultrashort laser: Lasing in MBE GaAs layer with perpendicular-to-film optical excitation and emission," *IEEE J. Quantum Electron.*, vol. QE-16, pp. 1283–1285, Dec. 1980.

[11] J. L. Jewell, Y. H. Lee, M. Warren, H. M. Gibbs, N. Peyghambarian, A. C. Gossard, and W. Wiegmann, "3-pJ, 82-MHz optical logic gates in a room-temperature GaAs-AlGaAs multiple- quantum-well etalon," *Appl. Phys. Lett.*, vol. 46, pp. 918–920, Jan. 1985.

[12] J. L. Jewell, K. F. Huang, K. Tai, Y. H. Lee, R. J. Fischer, S. L. McCall, and A. Y. Cho, "Vertical cavity single quantum well laser," *Appl. Phys. Lett.*, vol. 55, pp. 424–426, July 1989.

[13] J. L. Jewell, A. Scherer, S. L. McCall, A. C. Gossard, and J. H. English, "GaAs-AlAs monolithic microresonator arrays," *Appl. Phys. Lett.*, vol. 51, pp. 94–96, Apr. 1987.

[14] J. L. Jewell, S. L. McCall, Y. H. Lee, A. Scherer, A. C. Gossard, and J. H. English, "Lasing characteristics of GaAs microresonator lasers," *Appl. Phys. Lett.*, vol. 54, pp. 1400–1402, Apr. 1989.

[15] J. L. Jewell, S. L. McCall, A. Scherer, H. H. Houh, N. A. Whitaker, A. C. Gossard, and J. H. English, "Transverse modes, waveguide dispersion and 30 ps recovery in submicron GaAs/AlAs microresonator lasers," *Appl. Phys. Lett.*, vol. 55, pp. 22–24, July 1989.

[16] J. L. Jewell, A. Scherer, S. L. McCall, Y. H. Lee, S. J. Walker, J. P. Harbison, and L. T. Florez, "Low threshold electrically-pumped vertical cavity surface emitting micro-lasers," *Electron. Lett.*, vol. 25, pp. 1123–1124, Aug. 1989.

[17] Y. H. Lee, J. L. Jewell, A. Scherer, S. L. McCall, J. P. Harbison, and L. T. Florez, "Room-temperature continuous wave vertical cavity single quantum well microlaser diodes," *Electron. Lett.*, vol. 25, pp. 1377–1378, Sept. 1989.

[18] Y. H. Lee, J. L. Jewell, A. Scherer, B. Tell, K. Brown-Goebeler, J. P. Harbison, and L. T. Florez, "Effects of etch depth and ion implantation on surface emitting microlasers," *Electron. Lett.*, vol. 25, pp. 225–226, Feb. 1989.

[19] A. Scherer, J. L. Jewell, J. P. Harbison, and L. T. Florez, Y. H. Lee, and C. J. Sandroff, "Fabrication of low threshold CW electrically pumped surface emitting microlasers," *Appl. Phys. Lett.*, vol. 55, pp. 2724–2726, Dec. 1989.

[20] K. Y. Lau, P. L. Derry, and A. Yariv, "Ultimate limit in low threshold quantum well GaAlAs semiconductor lasers," *Appl. Phys. Lett.*, vol. 52, pp. 88–90, Jan. 1988.

[21] Y.-H. Wu, M. Ogura, M. Werner, and S. Wang, "New GaAlAs-GaAs surface emitting laser diodes with lateral pumping structure," *Electron. Lett.*, vol. 23, pp. 123–124, Jan. 1987.

[22] R. Geels, R. H. Yan, J. W. Scott, S. W. Corzine, R. J. Simes, and L. A. Coldren, "Analysis and design of a novel parallel-driven MQW-DBR surface-emitting-laser," in *CLEO '88 Tech. Dig.*, Opt. Soc. Amer., Anaheim, CA, May 1988.

[23] R. S. Geels, S. W. Corzine, J. W. Scott, D. B. Young, and L. A. Coldren, "Low threshold planarized vertical-cavity surface emitting lasers," *IEEE Photon. Technol. Lett.*, vol. 2, pp. 234–236, Apr. 1990.

[24] R. S. Geels and L. A. Coldren, "Submilliamp threshold vertical-cavity laser diodes," *Appl. Phys. Lett.*, vol. 57, pp. 1605–1607, Oct. 1990.

[25] M. Y. A. Raja, S. R. J. Brueck, M. Osinski, C. F. Schaus, J. G. McInerney, T. M. Brennan, and B. E. Hammons, "Surface-emitting multiple quantum well GaAs/AlGaAs laser with wavelength resonant periodic gain medium," *Appl. Phys. Lett.*, vol. 53, pp. 1678–1680, 1988.

[26] Y. H. Lee, B. Tell, K. F. Brown-Goebeler, J. L. Jewell, and J. V. Hove, "Top-surface-emitting GaAs four-quantum-well lasers emitting at 0.85 μm," *Electron. Lett.*, vol. 26, pp. 710–711, May 1990.

[27] Y. H. Lee, B. Tell, K. F. Brown-Goebeler, J. L. Jewell, R. E. Leibenguth, M. T. Asom, G. Livescu, L. Luther, and V. D. Mattera, "High efficiency (1.2 mW/mA) top surface-emitting GaAs quantum well lasers," *Electron. Lett.*, vol. 26, pp. 1308–1309, Sept. 1990.

[28] Y. H. Lee, B. Tell, K. F. Brown-Goebeler, J. L. Jewell, C. A. Burrus, and J. V. Hove, "Characteristics of top-surface-emitting GaAs lasers," *IEEE Photon. Technol. Lett.*, vol. 2, pp. 686–688, Sept. 1990.

[29] B. Tell, Y. H. Lee, K. F. Brown-Goebeler, J. L. Jewell, R. E. Leibenguth, M. T. Asom, G. Livescu, L. Luther, and V. D. Mattera, "High-power top surface-emitting GaAs quantum well lasers," *Appl. Phys. Lett.*, vol. 57, pp. 1855–1857, Oct. 1990.

[30] K. Tai, R. J. Fischer, K. W. Wang, S. N. G. Chu, and A. Y. Cho, "Use of implant isolation for fabrication of vertical cavity surface-emitting laser diodes," *Electron. Lett.*, vol. 25, pp. 1644–1645, Nov. 1989.

[31] M. Orenstein, A. C. von Lehman, C. Chang-Hasnain, N. G. Stoffel, J. P. Harbison, L. T. Florez, E. Clausen, and J. L. Jewell, "Vertical-cavity surface-emitting InGaAs/GaAs lasers with planar lateral definition," *Appl. Phys. Lett.*, vol. 56, pp. 2384–2386, June 1990.

[32] J. L. Jewell, Y. H. Lee, S. L. McCall, J. P. Harbison, and L. T. Florez, "High-finesse (Al,Ga)As interference filters grown by molecular beam epitaxy," *Appl. Phys. Lett.*, vol. 53, pp. 640–642, Aug. 1988.

[33] L. M. Zinkiewicz, T. J. Roth, L. J. Mawst, D. Tran, and D. Botez, "High-power vertical-cavity surface-emitting AlGaAs/GaAs diode lasers," *Appl. Phys. Lett.*, vol. 54, pp. 1959–1961, May 1989.

[34] K. Tai, L. Yang, Y. H. Wang, J. D. Wynn, and A. Y. Cho, "Drastic reduction of series resistance in doped semiconductor distributed Bragg reflector for surface emitting lasers," *Appl. Phys. Lett.*, vol. 56, pp. 2496–2498, June 1990.

[35] D. Botez, L. M. Zinkiewicz, T. J. Roth, L. J. Mawst, and G. Peterson, "Low-threshold-current-density vertical-cavity surface-emitting AlGaAs/GaAs diode lasers," *IEEE Photon. Technol. Lett.*, vol. 1, pp. 205–208, Aug. 1989.

[36] K. Tai, R. J. Fischer, C. W. Seabury, N. A. Olsson, T.-C. D. Huo, Y. Ota, and A. Y. Cho, "Room-temperature continuous wave vertical cavity surface emitting GaAs injection lasers," *Appl. Phys. Lett.*, vol. 55, pp. 2473–2475, Dec. 1989.

[37] E. F. Schubert, L. W. Tu, R. F. Kopf, G. J. Zydzik, and D. G. Deppe, "Low-threshold vertical cavity surface-emitting lasers with

metallic reflectors," *Appl. Phys. Lett.*, vol. 57, pp. 117–119, July 1990.
[38] J. I. Pankove, J. E. Berkeyheiser, S. J. Kilpatrick, and C. W. Magee, "Passivation of GaAs surfaces," *J. Electron. Material*, vol. 12, pp. 359–370, Mar. 1983.
[39] C. J. Sandroff, M. S. Hedge, L. A. Farrow, C. C. Chang, and J. P. Harbison, "Electronic passivation of GaAs surfaces through the formation of arsenic–sulfer bonds," *Appl. Phys. Lett.*, vol. 54, pp. 362–364, 1989.
[40] K. Tai, T. R. Hayes, S. L. McCall, and W. T. Tsang, "Optical measurement of surface recombination in InGaAs quantum well-mesa structures," *Appl. Phys. Lett.*, vol. 53, pp. 302–303, July 1988.
[41] T. Baba, T. Hamano, F. Koyama, and K. Iga, "Spontaneous emission factor in micro-cavity DBR surface emitting laser," Euro. Conf. Opt. Commun., Amsterdam, The Netherlands, Sept. 1990, postdeadline Paper ThG1.3.
[42] Y. Yamamoto, S. Machida, W. Richardson, K. Igeta, and G. Bjork, "Squeezing and cavity quantum electrodynamics in GaAs quantum well lasers," presented at the Int. Quantum Electron. Conf., Anaheim, CA, May 1990, Paper QWC6.
[43] E. Yablonovitch, T. J. Gmitter, and R. H. Bhat, "Inhibited and enhanced spontaneous emission from optically thin AlGaAs/GaAs double heterostructures," *Phys. Rev. Lett.*, vol. 61, pp. 2546–2549, Nov. 1988.
[44] S. Luryi, "Light emitting devices based on the real-space transfer of hot electrons," *Appl. Phys. Lett.*, vol. 58, pp. 1727–1729, Apr. 1991.
[45] A. Chailertvanitkul, K. Iga, and K. Moriki, "GaInAsP/InP surface emitting laser (λ = 1.4 μm, 77 K) with heteromultilayer Bragg reflector," *Electron. Lett.*, vol. 21, pp. 303–304, Mar. 1985.
[46] K. Tai, S. L. McCall, S. N. G. Chu, and W. T. Tsang, "Chemical beam epitaxially grown InP/InGaAsP interference mirror for use near 1.55 μm wavelength," *Appl. Phys. Lett.*, vol. 51, pp. 826–827, Sept. 1987.
[47] P. A. Morton, D. L. Crawford, and J. E. Bowers, "Design of 1.3 μm GaInAsP surface emitting lasers for high bandwidth operation," *Opt. Lett.*, vol. 15, pp. 679–681, 1990.
[48] D. G. Deppe, S. Singh, R. D. Dupuis, N. D. Gerrard, G. J. Zydzik, J. P. van der Ziel, C. A. Green, and C. J. Pinone, "Room-temperature photopumped operation of an InGaAs–InP vertical cavity surface-emitting laser," *Appl. Phys. Lett.*, vol. 56, pp. 2172–2174, May 1990.
[49] S. T. Ho, S. L. McCall, R . E. Slusher, L. N. Pfeiffer, K. W. West, A. F. J. Levi, G. E. Blonder, and J. L. Jewell, "High index contrast mirrors for optical microcavities," *Appl. Phys. Lett.*, vol. 57, pp. 1387–1389, Oct. 1990.
[50] D. M. Collins, "On the use of 'downward-looking' sources in MBE systems," *J. Vac. Sci. Technol.*, vol. 20, pp. 250–251, Feb. 1982.
[51] J. H. Neave, B. A. Joyce, P. J. Dobson, and N. Norton, "Dynamics of film growth of GaAs by MBE from RHEED oscillations," *Appl. Phys. A*, vol. 31, pp. 1–8, 1983.
[52] Y. H. Wang, K. Tai, Y. F. Hsieh, S. N. G. Chu, J. D. Wynn, and A. Y. Cho, "Observation of reduced current thresholds in GaAs/AlGaAs vertical-cavity surface emitting lasers grown on 4° off-orientation (001) GaAs substrates," *Appl. Phys. Lett.*, vol. 57, pp. 1613–1615, Oct. 15, 1990.
[53] A. Scherer, H. G. Craighead, M. L. Roukes, and J. P. Harbison, "Electrical damage induced by ion beam etching of GaAs," *J. Vac. Sci. Technol.*, vol. B6, pp. 227–279, Jan./Feb. 1988.
[54] A. Scherer and H. G. Craighead, "Fabrication of small laterally patterned multiple quantum wells," *Appl. Phys. Lett.*, vol. 49, pp. 1284–1286, 1986.
[55] A. Scherer, H. G. Craighead, and E. D. Beebe, "GaAs and AlGaAs reactive ion etching in BCl_3/Ar mixtures," *J. Vac. Sci. Technol.*, vol. B5, p. 1599, 1987.
[56] K. P. Giapis, G. R. Scheller, R. A. Gottscho, W. S. Hobson, and Y. H. Lee, "Microscopic and macroscopic uniformity control in plasma etching," *Appl. Phys. Lett.*, vol. 57, pp. 983–985, 1990.
[57] G. A. Lincoln, M. W. Geis, S. Pang, and N. Efremow, "Large area ion beam assisted etching of GaAs with high etch rates and controlled anisotropy," *J. Vac. Sci. Technol.*, vol. B1, pp. 1043, 1983.
[58] P. Grabbe, A. Scherer, K. Kash, R. Bhat, J. P. Harbison, L. T. Florez, and M. Koza, "Photoluminescence measurement of sidewall damage in etched InGaAsP/InP and GaAs/AlGaAs microstructures," *Material Res. Soc. Symp. Proc.*, vol. 144, p. 145, 1989.
[59] S. Pang, M. W. Geis, N. N. Efremow, and G. A. Lincoln, "Effects of ion species and adsorbed gas on dry etching induced damage in GaAs," *J. Vac. Sci. Technol.*, vol. B3, p. 398, 1985.
[60] A. Von Lehmen, C. Chang-Hasnain, M. Orenstein, J. Wullert, N. Stoffel, and J. P. Harbison, "Large electronically addressable VCSE laser arrays," presented at the Top. Meet. Opt. Multiple Access Networks, Monterey, CA, July 25–27, 1990.
[61] A. Von Lehmen, C. Chang-Hasnain, J. Wullert, L. Carrion, N. Stoffel, L. T. Florez, and J. P. Harbison, "Independently addressable InGaAs/GaAs VCSEL array," *Electron. Lett.*, vol. 27, pp. 583–595, Mar. 1991.
[62] M. Orenstein, A. C. Von Lehmen, C. Chang-Hasnain, N. G. Stoffel, J. P. Harbison, L. T. Florez, J. R. Wullert, and A. Scherer, "Matrix addressable surface emitting laser array (MASELA)," in *Proc. Opt. Soc. Amer. Annu. Meet.*, Orlando, FL, Oct. 16–20, 1989; see also, in *Proc. Conf. Lasers Electro-Opt. (CLEO '90)*, Anaheim, CA, May 21–25, 1990, Paper CTuF3; see also, *Electron. Lett.*, vol. 27, pp. 437–438, Feb. 1991.
[63] A. Von Lehmen, J. Wullert, M. Orenstein, C. Chang-Hasnain, N. Stoffel, L. T. Florez, and J. P. Harbison, "Statistics and rastered operation of row/column-addressed VCSE laser array," in *Proc. 1990 Annu. Meet. Opt. Soc. Amer.*, Boston, MA, Nov. 4–9, 1990; also, submitted to *IEEE Photon. Technol. Lett.*
[64] B. P. Van der Gaag and A. Scherer, "Microfabrication below 10 nm," *Appl. Phys. Lett.*, vol. 56, pp. 481–483, Jan. 1990.
[65] J. F. Ziegler, J. P. Biersack, and U. Littmark, *The Stopping and Range of Ions in Solids*, vol. 1. Elmsford, NY: Pergamon, 1984.
[66] H. K. Choi and C. A. Wang, "InGaAs/AlGaAs strained single quantum well diode lasers with extremely low threshold current density and high efficiency," *Appl. Phys. Lett.*, vol. 57, pp. 321–323, July 1990.
[67] F. S. Choa, Y. H. Lee, B. Tell, T. L. Koch, C. A. Burrus, J. L. Jewell, R. E. Leibenguth, and G. Boyd, "Dynamic characteristics of a high-performance vertical-cavity surface-emitting laser," presented at the Conf. Opt. Fiber Commun. '91, San Diego, CA, Feb. 18–22, 1991.
[68] C. J. Chang-Hasnain, J. P. Harbison, G. Hasnain, A. Von Lehmen, L. T. Florez, and N. G. Stoffel, "Dynamic polarization and transverse mode characteristics of vertical cavity surface emitting lasers," *IEEE J. Quantum Electron.*, this issue, , pp. 1368–1376.
[69] C. J. Chang-Hasnain, M. Orenstein, A. Von Lehmen, L. T. Florez, J. P. Harbison, and N. G. Stoffel, "Transverse characteristics of vertical cavity surface-emitting lasers," *Appl. Phys. Lett.*, vol. 57, pp. 218–220, July 1990.
[70] Y. C. Chung, private communication.
[71] J. C. Jeong, private communication.

Jack L. Jewell, photograph and biography not available at the time of publication.

J. P. Harbison, photograph and biography not available at the time of publication.

A. Scherer, photograph and biography not available at the time of publication.

Y. H. Lee, photograph and biography not available at the time of publication.

L. T. Florez, photograph and biography not available at the time of publication.